



1 **A Comparative Study of Two-way and**  
2 **Offline Coupled WRF v3.4 and CMAQ v5.0.2**  
3 **over the Contiguous U.S.: Performance**  
4 **Evaluation and Impacts of Chemistry-**  
5 **Meteorology Feedbacks on Air Quality**

6 Kai Wang<sup>1</sup>, Yang Zhang<sup>1\*</sup>, Shaocai Yu<sup>2\*</sup>, David C. Wong<sup>3</sup>, Jonathan Pleim<sup>3</sup>, Rohit Mathur<sup>3</sup>,  
7 James T. Kelly<sup>4</sup>, and Michelle Bell<sup>5</sup>

8 <sup>1</sup>Department of Civil and Environmental Engineering, Northeastern University, Boston, MA  
9 02115

10 <sup>2</sup>Key Laboratory of Environmental Remediation and Ecological Health, Ministry of Education;  
11 Research Center for Air Pollution and Health, College of Environment and Resource Sciences,  
12 Zhejiang University, Hangzhou, Zhejiang 310058, P.R. China

13 <sup>3</sup>Center for Environmental  
14 Measurement and Modeling, U.S. EPA, RTP, NC 27711

15 <sup>4</sup>Office of Air Quality Planning and Standards, U.S. EPA, RTP, NC 27711

16 <sup>5</sup>School of Forestry & Environmental Studies, Yale University, New Haven, CT 06511

17

18 *\*Correspondence to:* Yang Zhang (ya.zhang@northeastern.edu); Shaocai Yu (shaocaiyu@zju.edu.cn)

19



## 20 **Abstract**

21           The two-way coupled Weather Research and Forecasting and Community Multiscale Air  
22 Quality (WRF-CMAQ) model has been developed to more realistically represent the atmosphere  
23 by accounting for complex chemistry-meteorology feedbacks. In this study, we present a  
24 comparative analysis of two-way (with consideration of both aerosol direct and indirect effects)  
25 and offline coupled WRF v3.4 and CMAQ v5.0.2 over the contiguous U.S. Long-term (five-year  
26 of 2008-2012) simulations using WRF-CMAQ with both offline and two-way coupling modes  
27 are carried out with anthropogenic emissions based on multiple years of the U.S. National  
28 Emission Inventory and chemical initial and boundary conditions derived from an advanced  
29 Earth system model (i.e., a modified version of the Community Earth System Model/Community  
30 Atmospheric Model). The comprehensive model evaluations show that both two-way WRF-  
31 CMAQ and WRF-only simulations perform well for major meteorological variables such as  
32 temperature at 2 m, relative humidity at 2 m, wind speed at 10 m, and precipitation (except for  
33 against the National Climatic Data Center data) as well as shortwave/longwave radiation. Both  
34 two-way and offline CMAQ also show good performance for ozone (O<sub>3</sub>) and fine particulate  
35 matter (PM<sub>2.5</sub>). Due to the consideration of aerosol direct and indirect effects, two-way WRF-  
36 CMAQ shows improved performance over offline-coupled WRF and CMAQ in terms of  
37 spatiotemporal distributions and statistics, especially for radiation, cloud forcing, O<sub>3</sub>, sulfate,  
38 nitrate, ammonium, and elemental carbon as well as tropospheric O<sub>3</sub> residual and column  
39 nitrogen dioxide (NO<sub>2</sub>). For example, the mean biases have been reduced by more than 10 W m<sup>-2</sup>  
40 for shortwave radiation and cloud radiative forcing and by more than 2 ppb for max 8-h O<sub>3</sub>.  
41 However, relatively large biases still exist for cloud predictions, some PM<sub>2.5</sub> species, and PM<sub>10</sub>,  
42 which warrant follow-up studies to better understand those issues. The impacts of chemistry-



43 meteorological feedbacks are found to play important roles in affecting regional air quality in the  
44 U.S. by reducing domain-average concentrations of carbon monoxide (CO), O<sub>3</sub>, nitrogen oxide  
45 (NO<sub>x</sub>), volatile organic compounds (VOCs), and PM<sub>2.5</sub> by 3.1% (up to 27.8%), 4.2% (up to  
46 16.2%), 6.6% (up to 50.9%), 5.8% (up to 46.6%), and 8.6% (up to 49.1%), respectively, mainly  
47 due to reduced radiation, temperature, and wind speed. The overall performance of the two-way  
48 coupled WRF-CMAQ model achieved in this work is generally good or satisfactory and the  
49 improved performance for two-way coupled WRF-CMAQ should be considered along with other  
50 factors in developing future model applications to inform policy making.

51 **Keywords:** CMAQ, Two-way coupling, Evaluation, Chemistry-meteorology feedback

## 52 1. Introduction

53 The Community Multiscale Air Quality (CMAQ) modeling system developed by the U.S.  
54 Environmental Protection Agency (EPA) (Byun and Schere, 2006; Scheffe et al., 2016; San  
55 Joaquin Valley APCD, 2018; Pye et al., 2020; U.S. EPA, 2020) has been extensively used by  
56 both scientific community and governmental agencies over various geographical regions and  
57 under different meteorological and air pollution conditions to address major key air quality  
58 issues such as atmospheric ozone (O<sub>3</sub>), acid rain, regional haze, and trans-boundary or long-  
59 range transport of air pollutants during the past decades over North America (Zhang et al.,  
60 2009a,b; Wang and Zhang, 2012; Hogrefe et al., 2015), Asia (Wang et al., 2009, 2012; Liu et al.,  
61 2010; Zheng et al., 2015; Li et al., 2017; Xing et al., 2017; Yu et al., 2018; Mehmood et al.,  
62 2020), and Europe (Kukkonen et al., 2012; Mathur et al., 2017; Solazzo et al., 2017). The  
63 CMAQ model is traditionally driven offline by the three-dimensional meteorology fields  
64 generated separately from other meteorological models such as the Weather Research and  
65 Forecasting (WRF) model, and the dynamic feedbacks of chemistry predictions on meteorology



66 are neglected. However, more recently (IPCC, 2018), chemistry-meteorology feedbacks have  
67 been found to play important roles in affecting the both global and regional climate change and  
68 air quality (Jacobson et al., 1996; Mathur et al., 1998; Ghan et al., 2001; Zhang, 2008; Zhang et  
69 al., 2010, 2015a,b, 2017; Grell and Baklanov, 2011; Wong et al., 2012; Baklanov et al., 2014; Yu  
70 et al., 2014; Gan et al., 2015a; Wang et al., 2015; Xing et al., 2015a,b; Yahya et al., 2015a,b;  
71 Hong et al., 2017; Jung et al., 2019). Feedbacks of aerosols on radiative transfer through aerosol-  
72 radiation interactions (i.e., aerosol direct forcing) and aerosol-cloud interactions (i.e., aerosol  
73 indirect forcing) are especially important (Zhang, 2008; Zhang et al., 2015a,b; Baklanov et al.,  
74 2014; Wang et al., 2015; Yahya et al., 2015a,b). Recognizing this importance, as well as the  
75 recent advances in knowledge on chemistry-meteorology interactions and computational  
76 resources, the U.S. EPA developed a two-way coupled WRF-CMAQ model that accounts for the  
77 aerosol direct effect alone (Wong et al., 2012). This version of CMAQ has been applied for both  
78 regional and hemispheric studies (Wang et al., 2014; Hogrefe et al., 2015; Xing et al., 2016,  
79 2017; Hong et al., 2017, 2020; Sekiguchi et al., 2018; Yoo et al., 2019). For example, Xing et al.  
80 (2016) showed that aerosol direct feedbacks may further improve air quality resulting from  
81 emission controls in the U.S. and also indicated that coupled models are key tools for quantifying  
82 such feedbacks. Reduction in atmospheric ventilation resulting from aerosol induced surface  
83 cooling can exacerbate ground level air pollution. Hong et al. (2017) estimated an increase by  
84 4.8%-9.5% in concentrations of major air pollutants over China in winter due to incorporation of  
85 such effects. Xing et al. (2017) reported that the aerosol direct effects could reduce daily max 1h  
86 O<sub>3</sub> by up to 39 μg m<sup>-3</sup> over China in January through reducing solar radiation and photolysis  
87 rates. Hong et al. (2020) found that the benefits of reduced pollutant emissions through  
88 weakening aerosol direct effects can largely offset the additional deaths caused by the warming



89 effect of greenhouse gases over China. Some of those studies have also found that the missing  
90 aerosol indirect effects in WRF-CMAQ may introduce large model biases on their simulations of  
91 radiation and thus air quality (Wang et al., 2014; Sekiguchi et al., 2018; Yoo et al., 2019). There  
92 has been a growing awareness that both aerosol effects should be considered together to provide  
93 greater fidelity in coupling complex atmospheric processes among chemistry, aerosols, cloud,  
94 radiation, and precipitation (Grell and Baklanov, 2011). To address this issue and better represent  
95 the one-atmosphere modeling capability of CMAQ, Yu et al. (2014) further extended the two-  
96 way coupled WRF-CMAQ model by including aerosol indirect effects and improved WRF-  
97 CMAQ's capability for predicting cloud and radiation variables.

98 Different from the traditional online integrated air quality models such as the Gas,  
99 Aerosol, Transport, Radiation, General Circulation, and Mesoscale Meteorological (GATOR-  
100 GCMM) model (Jacobson, 2001), the WRF model coupled with chemistry (WRF/Chem; Grell et  
101 al., 2005) and the WRF model coupled with the Community Atmosphere Model version 5  
102 (WRF-CAM5; Ma et al., 2013; Zhang et al., 2015a,b; 2017), in which atmospheric dynamics and  
103 chemistry are integrated and simulated altogether without an interface between meteorology and  
104 atmospheric chemistry (Zhang et al., 2013), two-way WRF-CMAQ (also referred to as the online  
105 access model) is created by combining existing meteorology (i.e., WRF) and atmospheric  
106 chemistry (i.e., CMAQ) models with an interactive interface (Yu et al., 2014). As pointed out by  
107 Yu et al. (2014), the main advantage of two-way CMAQ is to allow the existing numerical  
108 techniques to be used in both WRF and CMAQ to facilitate future independent development of  
109 both models while also maintaining CMAQ as a stand-alone model (the offline capability). In the  
110 past, a number of studies have compared and evaluated online vs. offline-coupled model  
111 performance (Pleim et al, 2008; Matsui et al., 2009; Wilczak et al., 2009; Lin et al., 2010;



112 Herwehe et al., 2011; Yu et al., 2011; Wong et al., 2012; Zhang et al., 2013, 2016a; Choi et al.,  
113 2019). However due to the missing offline-coupled mode or component for most online-coupled  
114 models, many of those intercomparison studies are subject to some key limitations such as  
115 inconsistent model treatments in chemical options (Matsui et al., 2009; Lin et al., 2010; Zhang et  
116 al., 2013; Choi et al., 2019) or in both physical and chemical options (Wilczak et al., 2009;  
117 Herwehe et al., 2011; Zhang et al., 2016a), different domain projection methods or resolutions  
118 (Wilczak et al., 2009; Lin et al., 2010; Zhang et al., 2013), or disunified model inputs (Wilczak et  
119 al., 2009; Lin et al., 2010; Zhang et al., 2013). Due to the unique coupling approach, two-way  
120 WRF-CMAQ can be used to overcome those limitations and set up ideal intercomparisons  
121 between online and offline simulations using consistent model treatments (Pleim et al, 2008; Yu  
122 et al., 2011; Wong et al., 2012).

123 In this study, we provide a robust examination of model improvements by considering  
124 chemistry-meteorology feedbacks and their impacts on the U.S. air quality using the two-way  
125 WRF-CMAQ model (same version as in Yu et al., 2014) with both aerosol direct and indirect  
126 effects. Long-term (five-year of 2008-2012) simulations using both two-way and offline coupled  
127 WRF and CMAQ models are carried out and compared to the best of our knowledge for the first  
128 time over the contiguous U.S. (CONUS) with anthropogenic emissions based on multiple years  
129 of the U.S. National Emission Inventory (NEI) and chemical initial and boundary conditions  
130 (ICONS/BCONs) downscaled from the advanced Earth system model, i.e., an updated version of  
131 the Community Earth System Model/CAM5 (CESM/CAM5; He and Zhang, 2014; Glotfelty et  
132 al., 2017). Our objectives include 1) perform a comprehensive model evaluation for major  
133 meteorological variables and chemical species from this long-term application of the two-way



134 coupled WRF-CMAQ; and 2) conduct a comparative study of two-way and offline coupled WRF  
135 and CMAQ to examine the impacts of chemistry-meteorology interactions on U.S. air quality.

136           Compared to previous studies in the literature, there are a few key features of this work.  
137 First, the intercomparisons between two-way (or online) and offline WRF-CMAQ are performed  
138 here using consistent model configurations including both physical/chemical options and inputs.  
139 Second, unlike a few previous intercomparison studies (Pleim et al, 2008; Yu et al., 2011; Wong  
140 et al., 2012) using two-way WRF-CMAQ with only aerosol direct effects for relatively short  
141 episodes, the model version in this work includes both aerosol direct and indirect effects and  
142 simulations are conducted for multiple years to provide more robust assessments. Third,  
143 compared to other studies (e.g., Yahya et al., 2015a,b; Choi et al., 2019) focusing on the impacts  
144 of chemistry-meteorology feedbacks on meteorology only or limited chemical species, this study  
145 performs comprehensive and extensive evaluation and comparison to demonstrate importance of  
146 chemistry-meteorology feedbacks on regional meteorology and air quality.

## 147 **2. Model description, simulation setup, and evaluation protocols**

148           Two sets of five-year (i.e., 2008-2012) long-term simulations are conducted using the two-  
149 way coupled WRF v3.4-CMAQ v5.0.2 model with both aerosol direct and indirect effects and  
150 the sequentially offline-coupled WRF v3.4 and CMAQ v5.0.2 model, respectively, over the  
151 CONUS with 36-km horizontal grid spacing. The vertical resolution for these simulations  
152 consists of 34 layers from the surface (~38 m) to 100 hPa (~15 km). The two-way coupled WRF-  
153 CMAQ includes estimations of aerosol optical properties based on prognostic aerosol size  
154 distributions and composition . These aerosol optical properties are then used to modulate the  
155 shortwave radiation budget estimated using the Rapid and accurate Radiative Transfer Model for



156 General circulation (RRTMG) radiation scheme (Iacono et al., 2008) in WRF. Additionally,  
157 aerosol indirect effects, including the first (cloud albedo) and second (cloud lifetime) indirect  
158 aerosol forcing and the glaciation (ice and mixed-phase cloud lifetime) indirect aerosol forcing  
159 are also modeled. More details on the model development of this version of WRF-CMAQ can be  
160 found in Yu et al. (2014). On the other hand, the WRF only model calculates the radiation  
161 budgets by using prescribed aerosol optical properties such as aerosol optical depth, single  
162 scattering albedo and asymmetry parameters and cloud formation by assuming default droplet  
163 number concentration and fixed cloud effective radius, which may not be representative for the  
164 large regions with complex air pollution conditions. Both the two-way and offline coupled WRF-  
165 CMAQ use the same model configurations as shown in Table S1 in the supplementary material,  
166 except that prognostic aerosol impacts on radiation and clouds are fully treated in two-way  
167 WRF-CMAQ. The physics options include the RRTMG shortwave and longwave radiation  
168 schemes, the Asymmetric Convective Model (ACM2) planetary boundary layer (PBL) scheme  
169 (Pleim, 2007), the Pleim-Xiu (PX) land-surface scheme (Xiu and Pleim, 2001), the Morrison  
170 two-moment microphysics scheme (Morrison et al., 2009), and version 2 of the Kain–Fritsch  
171 (KF2) cumulus scheme (Kain, 2004). The chemical options include the Carbon Bond 2005  
172 (CB05) chemical mechanism (Yarwood et al., 2005) with additional chloride chemistry (Sarwar  
173 et al., 2008), the sixth generation CMAQ aerosol module (AERO6) (Appel et al., 2013), and  
174 CMAQ’s aqueous phase chemistry (AQCHEM). In addition, the time steps of dynamics and  
175 radiation for two-way WRF-CMAQ are set as 1 min and 15 mins, respectively, and the call  
176 frequency for CMAQ in the two-way coupled model is set to be 5 mins.

177 The meteorological ICONs/BCONs are generated from the National Centers for  
178 Environmental Prediction Final Analysis (NCEP-FNL) datasets and the chemical



179 ICONs/BCONs are downscaled from a modified version of CESMv1.2.2/CAM5 (He and Zhang,  
180 2014; Glotfelty et al., 2017). The anthropogenic emissions are based on two versions of NEI.  
181 NEI 2008 and NEI 2011 are used to cover the 5-year period, i.e., NEI 2008 for 2008-2010 and  
182 NEI 2011 for 2011-2012, respectively. Biogenic emissions are calculated online using the  
183 Biogenic Emissions Inventory System (BEIS) v3 (Schwede et al., 2005). The sea-salt and dust  
184 emissions are also generated online by CMAQ's inline modules (Zhang et al., 2005; Foroutan et  
185 al., 2017). Two-way coupled WRF-CMAQ simulations are reinitialized every 5 days to make  
186 meteorology simulations as accurate as possible while preserving the two-way chemistry-  
187 meteorology feedbacks. The WRF-only simulations that are used to drive the offline CMAQ  
188 simulations apply the same reinitialization method to be consistent with the two-way coupled  
189 WRF-CMAQ simulations.

190         The model evaluation in this work mainly focuses on the long-term climatological type of  
191 performance by comparing 5-year average spatially and temporally matched model predictions  
192 of major surface meteorological/radiation-cloud variables and surface/column chemical species  
193 against various surface/satellite observations and reanalysis data. The surface meteorological  
194 data include temperature at 2 m (T2), relative humidity at 2 m (RH2), wind speed at 10 m  
195 (WS10), and wind direction at 10 m (WD10) from the National Climatic Data Center (NCDC),  
196 and precipitation from the NCDC, the National Acid Deposition Program (NADP), the Global  
197 Precipitation Climatology Project (GPCP), the Parameter-elevation Regressions on Independent  
198 Slopes Model (PRISM), and the Tropical Rainfall Measuring Mission Multisatellite Precipitation  
199 Analysis (TMPA). The radiation and cloud data include downward shortwave radiation at the  
200 ground surface (SWDOWN), net shortwave radiation at the ground surface (GSW), downward  
201 longwave radiation at the ground surface (GLW), outgoing longwave radiation at the top of the



202 atmosphere (OLR), and shortwave and longwave cloud forcing (SWCF and LWCF) from the  
203 Clouds and the Earth's Radiant Energy System (CERES); aerosol optical depth (AOD), cloud  
204 fraction (CF), cloud water path (CWP), and cloud optical thickness (COT) from the MODerate  
205 resolution Imaging Spectroradiometer (MODIS); and cloud droplet number concentration  
206 (CDNC) derived based on MODIS data by Bennartz (2007). The chemical data include surface  
207 O<sub>3</sub> from the Aerometric Information Retrieval System-Air Quality Subsystem (AIRS-AQS) and  
208 the Clean Air Status and Trends Network (CASTNET); surface fine particulate matter (PM<sub>2.5</sub>)  
209 and its constituents including sulfate (SO<sub>4</sub><sup>2-</sup>), nitrate (NO<sub>3</sub><sup>-</sup>), ammonium (NH<sub>4</sub><sup>+</sup>), elemental  
210 carbon (EC), organic carbon (OC), and total carbon (TC = EC + OC) from the Interagency  
211 Monitoring of Protected Visual Environments (IMPROVE) and the Chemical Speciation  
212 Network (CSN); surface coarse particulate matter (PM<sub>10</sub>) from the AQS; and column abundance  
213 variables such as column carbon monoxide (CO) from the Measurements of Pollution in the  
214 Troposphere (MOPITT), tropospheric ozone residual (TOR) from the Ozone Monitoring  
215 Instrument (OMI), and column nitrogen dioxide (NO<sub>2</sub>) and formaldehyde (HCHO) from the  
216 Scanning Imaging Absorption Spectrometer for Atmospheric Chartography (SCIAMACHY).

217 The satellite datasets used in this study are all level-3 gridded monthly-averaged data  
218 with various resolutions (i.e., 0.25° for OMI and PRISM, 0.5° for SCIAMACHY, 1° for CERES,  
219 GPCP, MODIS, and MOPITT). For the calculation of model performance statistics, the satellite  
220 data with different resolutions are mapped to CMAQ's Lambert conformal conic projection  
221 using bi-linear interpolation in the NCAR command language. CMAQ model outputs at  
222 approximate time of the satellite overpass are paired with the satellite retrievals to facilitate a  
223 consistent comparison. Modeled CDNC is calculated as the average value of the layer of low-  
224 level warm clouds between 950 and 850 hPa as suggested by Bennartz (2007). Following the



225 approach of Wielicki et al. (1996), the SWCF and LWCF are calculated as the difference  
226 between the clear-sky and the all-sky reflected radiation at the top of atmosphere for both  
227 simulations and observations.

228 The statistical performance evaluation follows a protocol similar to that of Zhang et al.  
229 (2006, 2009a) and Yahya et al. (2016) and uses well-accepted statistical measures such as  
230 correlation coefficient (R), mean bias (MB), root mean square error (RMSE), normalized mean  
231 biases (NMB), and normalized mean error (NME) (S. Yu et al., 2006). Because of different  
232 sampling protocols among monitoring networks, the evaluation is conducted separately for  
233 individual networks for the same simulated variables/species.

### 234 **3. Comprehensive model evaluation of two-way WRF-CMAQ**

#### 235 **3.1 Meteorological evaluation**

##### 236 **3.1.1 Surface meteorological variables**

237 Figures 1a-d show the spatial distribution of 5-year average MBs for T2, RH2, WS10,  
238 and hourly precipitation from two-way WRF-CMAQ against the NCDC data in 2008-2012 and  
239 Table 1 summarizes the statistics for the same variables. All variables except for precipitation  
240 show overall good or moderate spatial performance with many sites showing MBs within  $\pm 0.6$   
241  $^{\circ}\text{C}$  for T2,  $\pm 5\%$  for RH2,  $\pm 1\text{ m s}^{-1}$  for WS10, and  $\pm 0.1\text{ mm hr}^{-1}$  for precipitation, respectively.  
242 WRF-CMAQ tends to overpredict T2 (i.e., warm bias) over widespread areas of domain  
243 especially along the Atlantic coast, the eastern/southeastern U.S., the Central U.S., and Pacific  
244 coast. The model also shows cold biases (i.e., underprediction in T2) over the mountainous  
245 regions and northeastern U.S. Similar warm biases of T2 have been previously reported by  
246 Cohen et al. (2015) and are found to be associated with the relatively deeper PBL depth using the



247 non-local ACM2 PBL scheme. The relatively larger warm/cold biases over coastal and  
248 mountainous areas are likely caused by the coarse spatial grid spacing of 36-km which cannot  
249 resolve the complex topography. Compared to many previous WRF studies (Wang et al., 2012;  
250 Brunner et al., 2015; Yahya et al., 2016), which typically show cold T2 biases, the overall small  
251 warm biases in this study can be attributed to the soil moisture nudging technique used in the PX  
252 land surface scheme (Pleim and Gilliam, 2009). The spatial patterns of MBs for RH2 show a  
253 clear anti-correlation compared to T2 (i.e., RH2 is overpredicted where T2 is underpredicted and  
254 vice versa). This is consistent with how RH2 is calculated based on T2. The spatial distribution  
255 of MBs for WS10 also shows dominant overpredictions especially along coastlines, indicating  
256 the prescribed sea-surface temperature might not be sufficient to resolve the air-sea interactions.  
257 Systematic overpredictions of hourly precipitation against NCDC data are found to be mainly  
258 caused low non-convective precipitation events and should be attributed to the uncertainties  
259 associated with the Morrison microphysics scheme (Yahya et al., 2016).

260         The precipitation performance is further examined by comparing WRF-CMAQ with  
261 GPCP and PRISM as shown in Figures 1e-g. The spatial distribution of precipitation is well  
262 simulated by WRF-CMAQ especially over the land against both GPCP and PRISM by capturing  
263 the hot spots along the Pacific Northwest coast and some areas over eastern U.S. Moderate  
264 overpredictions of precipitation against GPCP over the Atlantic Ocean and Gulf of Mexico are  
265 also evident, possibly due to overprediction of convective precipitation intensity by the Kain–  
266 Fritsch cumulus scheme (Hong et al., 2017) over ocean. As shown in Table 1, the domain-  
267 average statistics demonstrate good performance for all variables except for precipitation against  
268 NCDC in terms of MBs, NMBs, RMSE, and Rs. For example, the MBs for T2, RH2, WS10, and  
269 precipitation are 0.1 °C, 2.2%, 0.44 m s<sup>-1</sup>, and 0.14-0.28 mm day<sup>-1</sup>, respectively, and Rs for those



270 variables are typically between 0.5-0.98, which are well within the performance benchmark  
271 values recommended by Zhang et al. (2013) and Emery et al. (2017).

### 272 **3.1.2 Radiation and cloud variables**

273 Figure 2 compares the 5-year average spatial distribution of major radiation variables  
274 (i.e., SWDOWN, GSW, GLW, OLR, and AOD) based on the satellite retrievals and two-way  
275 WRF-CMAQ simulations, and Table 1 summarizes the domain-average model performance  
276 statistics. WRF-CMAQ predicts the longwave radiation variables GLW and OLR very well with  
277 domain-average of NMBs of -1.9% and 0.8%, respectively, and Rs of 0.99 for both. The  
278 shortwave radiation variables SWDOWN and GSW are overpredicted on average with NMBs of  
279 13.0% and 11.1%, respectively, and Rs of 0.97 for both. The simulations also reliably reproduce  
280 the spatial distribution of both longwave and shortwave radiation compared to observations. The  
281 relatively large overpredictions for shortwave radiation are very likely caused by the  
282 underpredictions of aerosol direct radiative forcing reflected from the underpredictions of AOD  
283 (Figure 2) as well as underprediction of indirect cloud radiative forcing (see Figure 3). It has  
284 been reported that WRF v3.4 does not treat the subgrid cloud feedback to radiation, which could  
285 also contribute to the overpredictions in shortwave radiation (Alapaty et al., 2012; Hong et al.,  
286 2017). The model largely underpredicts the magnitude of AOD (NMB: -64.8%), while providing  
287 a reasonable representation of the spatial distribution of AOD over the U.S., with generally  
288 higher values in the east and lower values in the west. The model also underpredicts the elevated  
289 AODs over oceans and the northern part of domain. Similar AOD underpredictions have been  
290 reported in previous studies over the U.S. using two-way coupled WRF-CMAQ (Gan et al.,  
291 2015a; Hogrefe et al., 2015; Xing et al., 2015a). The relatively large underpredictions of AOD  
292 may be caused by several factors. First, underprediction of PM<sub>2.5</sub> concentrations, particularly



293  $\text{SO}_4^{2-}$  and OC (Table 2), can contribute significantly to the underprediction of AOD, especially  
294 over the eastern U.S. Second, the underestimation of dust emissions may contribute to missing  
295 hot spots from the model over arid areas in CA and AZ (Foroutan et al., 2017) and  
296 underestimates of sea-salt emissions may lead to missing elevated AODs over oceans (Gan et al.,  
297 2015b). Third, challenges in adequately representing prescribed and wildfire emissions in the  
298 NEI (Kelly et al., 2019) may cause many missing hot spots over large areas of the Pacific  
299 Northwest, CA, Canada, and the eastern U.S. Fourth, uncertainties in BCONs of  $\text{PM}_{2.5}$   
300 concentrations may further contribute to underpredictions of AOD over oceans and the northern  
301 part of the domain. For example, Kaufman et al. (2001) found that the background AOD could  
302 reach 0.1 over the Pacific Northwest using Aerosol Robotic Network (AERONET) data. The  
303 AODs in the current simulation seem to be biased low (between 0.06-0.08) and indicate potential  
304 underpredictions of  $\text{PM}_{2.5}$  BCONs, especially in the free troposphere. Finally, there are  
305 uncertainties associated with MODIS retrievals. Remer et al. (2005) found that the uncertainty of  
306 level 3 MODIS monthly AODs can be up to  $\pm 0.05 \pm 0.15 \text{AOD}$  over the land due to clouds and  
307 surface reflectance. More AOD data from other satellites or AERONET might be considered in  
308 the future work to provide more robust ensemble type of evaluation for AOD.

309 Figures 3 and 4 compare the 5-year average spatial distribution of major cloud and cloud  
310 radiative variables for the satellite retrievals and two-way WRF-CMAQ simulations, and Table 1  
311 summarizes the domain-average model performance statistics. As shown in Figure 3, WRF-  
312 CMAQ tends to largely underpredict CDNC, COT, and CWP over the whole domain with the  
313 domain-average NMBs of -82.1%, -80.1%, and -51.2%, respectively. Despite the large  
314 underprediction of those cloud variables, the spatial correlations are generally predicted well,  
315 especially for COT and CWP with  $R_s$  of 0.84 and 0.79, respectively. Compared to the other



316 cloud variables, CF is much better predicted with an NMB of -12.2% and an R of 0.92, which is  
317 consistent with the performance reported in Yu et al. (2014). The model can reproduce the high  
318 CFs over northern and northeastern part of domain as well as over oceans while capturing the  
319 low CFs over the mountainous and plateau regions in the U.S. and Mexico. In addition to the  
320 underprediction of  $PM_{2.5}$  (thus underestimating CCN), the large underpredictions of cloud  
321 variables (especially CDNC and COT) can be attributed to uncertainties in aerosol microphysics  
322 schemes (Yahya et al., 2016) as well as missing aerosol indirect effects on subgrid convective  
323 clouds (Yu et al., 2014). Gantt et al. (2014) and Zhang et al. (2015b) also showed the aerosol  
324 activation scheme (i.e., Abdul-Razzak and Ghan, 2000) used in the current version of WRF-  
325 CMAQ may have underestimated CDNC and thus CWP and COT due to some missing processes  
326 such as insoluble aerosol adsorption and giant cloud condensation nuclei. Overall, the relatively  
327 poor model performance for cloud variables reflects current limitations in representing aerosol  
328 indirect effects and aerosol-cloud interactions in state-of-science online coupled models. Further  
329 model improvements that incorporate new knowledge from emerging studies should be  
330 conducted in the future.

331 As shown in Figure 4, WRF-CMAQ predictions of SWCF and LWCF agree well with the  
332 satellite-based values. The model partially captures the elevated SWCF and LWCF over the  
333 Atlantic Ocean, Pacific Northwest, and widespread areas over the eastern U.S. The domain-  
334 average NMBs are -26.0% for SWCF and -22.2% for LWCF, respectively. As discussed earlier,  
335 the underpredictions of SWCF may partially contribute the overprediction of SWDOWN (more  
336 shortwave radiation reaching the ground) and those of LWCF may further lead to the  
337 overpredictions in OLR (more longwave radiation emitted into the space). The performance of  
338 SWCF and LWCF is consistent with the 12-km simulation reported in Yu et al. (2014) and even



339 slightly better in terms of NMBs, which might be associated with the long-term vs. short-term  
340 simulations. It is also worth noting that SWCF (LWCF) is calculated as the difference between  
341 the clear-sky and all-sky shortwave (longwave) radiation at the top of atmosphere, and so  
342 performance for SWCF and LWCF depends on performance for both radiation and cloud  
343 properties. The generally better performance in terms of model bias for SWCF and LWCF  
344 compared to the cloud variables seems to be driven by the relatively good performance of  
345 shortwave/longwave radiation in the model.

## 346 **3.2 Chemical evaluation**

### 347 **3.2.1 O<sub>3</sub>**

348 Figure 5a shows the spatial distribution of simulated average daily maximum 8-h O<sub>3</sub> from  
349 two-way WRF-CMAQ overlaid with observations from both the AIRS-AQS and CASTNET  
350 networks. WRF-CMAQ shows good performance by capturing the spatial distribution of max 8-  
351 h O<sub>3</sub> over widespread areas of the domain. The model tends to overpredict O<sub>3</sub> along coastlines in  
352 the southeastern U.S., Gulf of Mexico, and Pacific coast, which can be attributed to a poor  
353 representation of coastal boundary layers (Yu et al., 2007), the warm T2 biases as shown in  
354 Figure 1, and lack of O<sub>3</sub> sink via halogen chemistry (Sarwar et al., 2015) and deposition to water  
355 (Gantt et al., 2017). The simulation also underpredicts O<sub>3</sub> in widespread areas in the Midwest,  
356 eastern, and mountainous regions of the U.S., which is consistent with the results of 36-km  
357 simulations from Wang and Zhang (2012) that used an earlier version of CMAQ v4.6 with the  
358 same CB05 gas-phase mechanism. In addition to cold T2 biases over those areas (Figure 1), the  
359 underpredictions are also believed to be associated with inaccurate representations of precursor  
360 emissions and elevated/complex terrain due to the coarse grid spacing of 36-km over those



361 regions. Wang and Zhang (2012) found that their 12-km simulation showed improved  
362 performance over similar regions.

363 Figure 5c shows the monthly variation of domain-average 5-year average O<sub>3</sub> mixing  
364 ratios between observations from AIRS-AQS and simulations from two-way WRF-CMAQ, and  
365 Figure 5d shows the diurnal variation of domain-average 5-year average hourly O<sub>3</sub> mixing ratios  
366 between observations from CASTNET and simulations from two-way WRF-CMAQ for  
367 representative winter (DJF and blue color) and summer (JJA and red color) seasons. As shown in  
368 Figure 5c, the O<sub>3</sub> mixing ratios are overpredicted throughout the year, which is consistent with  
369 overprediction of T<sub>2</sub> (figure not shown). The largest overprediction occurs in the relatively cold  
370 months such as September to December. It is interesting that the observations show the largest  
371 monthly O<sub>3</sub> mixing ratios in spring and early summer while the simulation shows the peak  
372 during the summer. The difference in timing of peak O<sub>3</sub> between observations and simulations  
373 during the year might be associated with uncertainties in the BCONs of O<sub>3</sub> that reflect impacts of  
374 the long-range transport and associated stratosphere-troposphere exchange of O<sub>3</sub>. As shown in  
375 Figure 5d, WRF-CMAQ tends to overpredict O<sub>3</sub> during most hours (i.e., 2:00-18:00) in summer  
376 and throughout the whole day in winter partially due to the overprediction of T<sub>2</sub>, especially in  
377 winter (figure not shown). The diurnal pattern of O<sub>3</sub> is captured much better during summer with  
378 much less prediction bias, especially during the nighttime, indicating that the model does a better  
379 job in predicting the evolution of nocturnal boundary layer and atmospheric chemistry in the  
380 warm season than the cold season. The overall overpredictions in this work are also consistent  
381 with previous studies (Eder and Yu, 2006; Appel et al., 2007; Wang et al., 2012), although our  
382 results show much better nighttime performance owing to the application of the ACM2 scheme  
383 that treats both local and non-local closure (Pleim, 2007). As also shown in Table 2, the domain-



384 average NMBs and NMEs for max 8-h O<sub>3</sub> are 12.6% and 13.1% against AIRS-AQS and 1.5%  
385 and 8.4% against CASTNET, respectively. The statistics are also consistent with previous  
386 studies using the CMAQ model (Zhang et al., 2009a; Appel et al., 2013, 2017; Penrod et al.,  
387 2014) and can be considered as good performance according to the criteria suggested by Zhang  
388 et al. (2013) and Emery et al. (2017).

### 389 **3.2.2 Aerosols**

390 Figure 6a shows the spatial distribution of simulated 5-year average PM<sub>2.5</sub> from two-way  
391 WRF-CMAQ overlaid with observations from both the CSN and IMPROVE networks, and  
392 Figure S1 shows the spatial distribution of the major PM<sub>2.5</sub> constituents overlaid with  
393 observations from the CSN and IMPROVE network and PM<sub>10</sub> overlaid with observations from  
394 the AQS network. As shown, WRF-CMAQ performs well for PM<sub>2.5</sub> over widespread areas of the  
395 Midwest and northeastern U.S., while PM<sub>2.5</sub> is underpredicted over the southeastern and western  
396 U.S. The model also misses some hot spots of observed concentrations in the western U.S.,  
397 which are mainly caused by TC underpredictions (Figure S1) that are likely linked to poorly  
398 allocated and underestimated wildfire emissions in the NEI (Wiedinmyer et al., 2006; Roy et al.,  
399 2007; Kelly et al., 2019). The relatively large underpredictions over the eastern U.S. are mainly  
400 caused by the combined effects from SO<sub>4</sub><sup>2-</sup>, NH<sub>4</sub><sup>+</sup>, and TC. As shown in Figure S1, WRF-CMAQ  
401 largely underpredicts SO<sub>4</sub><sup>2-</sup> in the Midwest and southeastern U.S. mainly due to the  
402 underprediction of oxidants such as O<sub>3</sub> (see Figure 5a) (which leads to less production from the  
403 gaseous oxidation), overprediction of precipitation (see Figure 1d) (which leads to more wet  
404 deposition and removal), and large underprediction of cloud fields (see Figure 3) (which leads to  
405 less aqueous phase formation), over the same area. On the other hand, NH<sub>4</sub><sup>+</sup> and NO<sub>3</sub><sup>-</sup> are either  
406 underpredicted or overpredicted, respectively, over the similar areas mainly due to



407 underprediction of  $\text{SO}_4^{2-}$ . According to the aerosol thermodynamics, when  $\text{SO}_4^{2-}$  is  
408 underpredicted,  $\text{NH}_4^+$  tends to be underpredicted due to its major role as cation. More gaseous  
409  $\text{NH}_3$  will be available to neutralize  $\text{NO}_3^-$ , thus leading to overprediction of  $\text{NO}_3^-$  especially over  
410 the sulfate poor regions (West et al., 1999). Other potential reasons include the inaccurate  
411 assumptions in the thermodynamic module (for example, the internally mixed aerosol state and  
412 equilibrium assumption may not be representative over some regions and different time periods,  
413 S. Yu et al., 2006), uncertainties in emissions of key species such as  $\text{NH}_3$  and non-volatile  
414 cations that affect particle acidity (Mebust et al., 2003; Wang and Zhang, 2014; Vasilakos et al.,  
415 2018; Pye et al., 2020), and measurement errors especially for  $\text{NO}_3^-$  and  $\text{NH}_4^+$  (X.-Y. Yu et al.,  
416 2006; Karydis et al., 2007; Wang and Zhang, 2012). TC underpredictions over most sites of the  
417 domain can be attributed to the underprediction of emissions (e.g., wildfire and primary OC) and  
418 underestimation of secondary organic aerosol (SOA) formation (Appel et al., 2017; Pye et al.,  
419 2017) since EC (a chemically inert species) is overpredicted, which suggest that atmospheric  
420 mixing did not drive the TC underpredictions. Figures 6e-6h show the scatter plots of major  
421  $\text{PM}_{2.5}$  components such as  $\text{SO}_4^{2-}$ ,  $\text{NH}_4^+$ , and  $\text{NO}_3^-$ , and TC. The WRF-CMAQ predicts  $\text{PM}_{2.5}$   
422 constituents well with the majority of data within the 1:2 ratio lines. Systematic underpredictions  
423 of  $\text{SO}_4^{2-}$  and  $\text{NH}_4^+$  and overpredictions of  $\text{NO}_3^-$  are shown, which are consistent with their spatial  
424 distributions. Relatively large under- and overpredictions of TC compensate each other and lead  
425 to relatively low overall model biases. As also shown in Figure S1, the model fails to reproduce  
426 high concentrations of  $\text{PM}_{10}$  (those  $> 20 \mu\text{g m}^{-3}$ ) over widespread areas of the domain, especially  
427 over dust source areas in CA, AZ, and NM. Hong et al. (2017) found the similar large  
428 underprediction of dust using CMAQ v5.0.2 over China and attributed it to a too-high threshold  
429 for friction velocity in the current dust module (Dong et al., 2016). Sea-salt also seems to be



430 underpredicted by WRF-CMAQ, although sea-salt predictions are better than dust as shown  
431 along the coastlines.

432           Figures 6c and 6d show the monthly variation of 5-year average  $PM_{2.5}$  between  
433 observations from CSN and IMPROVE, respectively, and simulations from two-way WRF-  
434 CMAQ. Both observations and WRF-CMAQ show higher monthly  $PM_{2.5}$  concentrations at CSN  
435 sites than IMPROVE sites throughout the year because most CSN sites are in more polluted  
436 urban areas while IMPROVE sites are in rural areas and national parks. The model tends to  
437 underpredict  $PM_{2.5}$  over both CSN and IMPROVE sites in the warm months (i.e., April to  
438 September) mainly due to the underpredictions of  $SO_4^{2-}$  and OC while it overpredicts  $PM_{2.5}$  in  
439 cold months mainly due to  $NO_3^-$ . The model also captures the seasonality of  $PM_{2.5}$  better over  
440 CSN sites than IMPROVE sites, especially in the summer months. The large underpredictions  
441 over IMPROVE sites during summer months are likely due to the underestimation of precursor  
442 emissions (such as wildfire emissions).

443           There are no universally accepted performance criteria for aerosols. As recommended by  
444 some previous studies (Zhang et al., 2006; Wang and Zhang, 2012), generally  $\pm 15\%$  and  $\pm 30\%$   
445 for model biases and 30% and 50% for model errors can be considered as good and acceptable  
446 performance. As shown in Table 2, WRF-CMAQ in this work demonstrates an overall good or  
447 acceptable performance in predicting aerosols in terms of statistics especially for  $PM_{2.5}$ ,  $NO_3^-$ ,  
448  $NH_4^+$ , and TC. It shows the domain-average NMBs of -7.0% and -13.7% for  $PM_{2.5}$  against CSN  
449 and IMPROVE, respectively; NMBs of -26.7% and -27.2% for  $SO_4^{2-}$  against CSN and  
450 IMPROVE, respectively; NMBs of 16.6% and 14.6% for  $NO_3^-$  against CSN and IMPROVE,  
451 respectively; an NMB of -14.3% for  $NH_4^+$  against CSN; NMBs of 20.6% and 29.4% for EC  
452 against CSN and IMPROVE, respectively; an NMB of -28.9% for OC against IMPROVE; and



453 NMBs of -9.4% and -9.2% for TC against CSN and IMPROVE, respectively. The relatively  
454 large underpredictions of PM<sub>10</sub>, i.e., an NMB of -45.9% against AQS, indicate further  
455 improvements of dust emissions are warranted. Overall, the aerosol performance is also  
456 comparable or better than previous CMAQ or WRF-CMAQ applications (Wang and Zhang,  
457 2012; Penrod et al., 2014; Yu et al., 2014). For example, Penrod et al. (2014) showed 5-year  
458 (2001-2005) summer mean NMBs of -19.1% to -17.6% for PM<sub>2.5</sub> against CSN and IMPROVE  
459 data over the CONUS using the CMAQ v5.0 and Yu et al. (2014) reported the monthly mean  
460 NMBs of -6.2% and -16.8% for PM<sub>2.5</sub> against CSN and IMPROVE over the eastern U.S. using  
461 the same version of WRF-CMAQ as that used in this study.

### 462 3.2.3 Column abundance

463 Figure 7 shows the spatial distribution of 5-year average column abundances between  
464 various satellite products and two-way WRF-CMAQ for column CO, TOR, column NO<sub>2</sub>, and  
465 column HCHO, and Table 2 summarizes the statistics. As shown, WRF-CMAQ can reproduce  
466 the spatial distribution of the column abundances of gases quite well with Rs ranging from 0.83  
467 to 0.91. TOR, column NO<sub>2</sub> and column HCHO are also generally well predicted in terms of  
468 magnitude with NMBs of 1.6%, -14.5%, and 18.0%, respectively. Systematic underpredictions  
469 for column CO occur over the whole domain with an NMB of -26.6% for a few reasons. First,  
470 the BCONs of CO may be significantly underestimated from the CESM model. Using  
471 WRF/Chem or its variant, Zhang et al. (2016b, 2019) found that the column CO performance  
472 could be greatly improved by adjusting the BCON using the satellite observation. A similar  
473 approach could be applied in future WRF-CMAQ simulations as well. Second, as pointed by  
474 Heald et al. (2003), the regional emissions, especially biomass burning, could be a significant  
475 source for elevated CO concentrations and thus underestimation of these emissions could



476 contribute to the CO underprediction. A more robust set of fire emissions from FINN generated  
477 by NCAR based on satellite retrievals has been applied to the similar time period recently but  
478 using the WRF-Chem model (Zhang and Wang, 2019) and were found to improve the CO  
479 performance. Last, Emmons et al. (2009) showed positive biases (i.e., 19%) of MOPITT  
480 retrievals over the land when compared to in-situ measurements and the biases may have been  
481 increasing over time due to the MOPITT bias drift (e.g.,  $0.5\% \text{ yr}^{-1}$  for version 7 retrieval). The  
482 predicted TOR can capture the observed high values over the eastern U.S. and oceans and the  
483 low values in elevated terrain; and it shows the best performance among all gas species. Both  
484 satellite observations and simulations can capture the elevated column  $\text{NO}_2$  over the industrial  
485 and metropolitan areas in the domain where large nitrogen oxide ( $\text{NO}_x$ ) emission sources are  
486 located. The model shows moderate underprediction which can be attributed to both  
487 uncertainties in the emissions and satellite retrievals. For example, the lightning emissions of  
488  $\text{NO}_x$  are missing from this study, which have been found by previous studies (Allen et al., 2012)  
489 to contribute up to  $2.0 \times 10^{15}$  molecules  $\text{cm}^{-2}$  over the southern U.S., the Gulf of Mexico, and  
490 northern Atlantic Ocean during certain episodes. Boersma et al. (2004) also found that different  
491 column  $\text{NO}_2$  retrieval approaches may lead to large errors ( $> 25\%$ ) over polluted areas. Column  
492 HCHO over the CONUS especially the southeastern U.S. is well predicted in terms of magnitude  
493 and spatial distribution and correlates well with the biogenic emission source regions. The  
494 underprediction of column HCHO may thus indicate potential underestimation of biogenic  
495 emissions from the BEIS. Other reasons including potential low yield of HCHO from isoprene  
496 and terpene in the CB05 mechanism and uncertainties in satellite retrievals (Stavrakou et al.,  
497 2009; Lorente et al., 2017)

#### 498 **3.2.4 Simulated $\text{O}_3$ and $\text{PM}_{2.5}$ exceedances of NAAQS levels**



499 National Ambient Air Quality Standards (NAAQS) are set for criteria pollutants,  
500 including O<sub>3</sub> and PM<sub>2.5</sub>, to provide protection against adverse health and welfare effects  
501 ([www.epa.gov/criteria-air-pollutants/naaqs-table](http://www.epa.gov/criteria-air-pollutants/naaqs-table)). In this section, the average number of days  
502 per year where the 24-hr PM<sub>2.5</sub> NAAQS level (35 µg m<sup>-3</sup>) and the max 8-h O<sub>3</sub> NAAQS level (70  
503 ppb) are exceeded from the WRF-CMAQ predictions is compared with the number of  
504 exceedances in the monitoring data (i.e., O<sub>3</sub> from AQS and CASTNET and PM<sub>2.5</sub> from  
505 IMPROVE and CSN). This comparison is intended to better characterize the ability of the model  
506 to simulate the high-concentration days that could be especially relevant in regulatory  
507 assessments. In Figure 8, the five-year average of the annual number of exceedance days is  
508 shown for WRF-CMAQ and the monitoring data at monitor locations. The sizes of circles and  
509 shades of color represent the magnitude of exceedances (i.e., larger circles and darker shades  
510 indicate a greater number of exceedance days). As shown, the observations indicate a large  
511 number of annual exceedance days for max 8-h O<sub>3</sub> over major cities, especially in CA, TX, the  
512 Midwest, and northeastern U.S. The spatial distribution of the observed number of exceedance  
513 days from the AQS and CASTNET networks aligns well with the nonattainment map reported by  
514 the Green Book of U.S. EPA (<https://www.epa.gov/green-book>). The WRF-CMAQ model also  
515 generally captures the distribution of the number of exceedance days very well, especially in CA.  
516 The domain-average values of NMB, NME, and R are -3.4%, 14.0%, and 0.98, respectively, also  
517 indicating a good performance. For PM<sub>2.5</sub>, the largest number of exceedance days based on the  
518 IMPROVE and CSN observations mainly occurs in the northwestern U.S., Midwest, and major  
519 cities in the northeastern U.S. The number of exceedance days is generally much lower for PM<sub>2.5</sub>  
520 than O<sub>3</sub>. The spatial distribution of the number of exceedance days for observed PM<sub>2.5</sub> aligns  
521 well with nonattainment areas reported by the Green Book from U.S. EPA in CA. However, the



522 number of simulated PM<sub>2.5</sub> exceedance days underpredicts the observation-based values in the  
523 western U.S. mainly due to large underpredictions of PM<sub>2.5</sub> concentrations in the same areas as  
524 shown in Figure 6a. The simulation better predicts the distribution of the number of exceedance  
525 days in the eastern U.S. where terrain is relatively flat and wildfire less prevalent. The domain-  
526 average values of NMB, NME, and R are -29.0%, 80.8%, and 0.21, respectively.

#### 527 **4. Impacts of chemistry-meteorology feedbacks**

528 In this section, the impacts of chemistry-meteorology feedbacks including aerosol direct  
529 and indirect effects on regional meteorology and air quality over the U.S. are further examined  
530 by comparing results from two-way WRF-CMAQ and offline coupled WRF and CMAQ. Model  
531 performance from the two sets of simulations is first compared to demonstrate the potential  
532 performance improvements of the two-way model, and the impacts on regional meteorology and  
533 air quality are further investigated via the spatial difference plots for selected variables and  
534 species.

#### 535 **4.1 Meteorology**

536 Figures 1 and 4 compare observations and simulations from the two-way WRF-CMAQ  
537 and WRF-only models for precipitation and SWCF/LWCF, respectively. Table 1 also  
538 summarizes the model performance statistics for all major meteorological variables for the two  
539 simulations. The statistics of some cloud variables from the WRF-only simulation are not  
540 available due to missing model outputs. Overall, good performance is evident for both  
541 simulations for surface meteorological variables with slightly better performance (except for  
542 RH2) for the two-way WRF-CMAQ simulation than the WRF-only simulation. The MBs for the  
543 two-way WRF-CMAQ vs. WRF-only simulation are 0.1°C vs 0.2 °C for T2, 2.2% vs 1.8% for



544 RH2,  $0.44 \text{ m s}^{-1}$  vs  $0.46 \text{ m s}^{-1}$  for WS10, 32.8 degree vs 33.4 degree for WD10, and 0.14-0.71  
545  $\text{mm day}^{-1}$  vs 0.2-0.8  $\text{mm day}^{-1}$  for precipitation. The spatial distributions for SWCF and LWCF  
546 are slightly better captured especially over the Midwest, Atlantic Ocean, and Pacific Northwest  
547 regions. Compared to WRF-only, two-way WRF-CMAQ shows noticeably better performance in  
548 terms of both MB and RMSE for radiation and cloud forcing, with MBs of  $37.0$  vs.  $24.2 \text{ W m}^{-2}$   
549 for SWDOWN,  $28.5$  vs  $17.6 \text{ W m}^{-2}$  for GSW,  $-10.6$  vs.  $-6.1 \text{ W m}^{-2}$  for GLW,  $2.8$  vs.  $2.0 \text{ W m}^{-2}$   
550 for OLR,  $-17.6$  vs.  $-10.7 \text{ W m}^{-2}$  for SWCF, and  $-5.9$  vs.  $-5.3 \text{ W m}^{-2}$  for LWCF. These results are  
551 consistent with those reported by Yahay et al. (2015a,b) that showed similar improvements in  
552 meteorological and radiative variables when comparing predictions from WRF-Chem with those  
553 from WRF only. Since identical inputs and physics options are used in both simulations, the  
554 differences in performance for meteorological variables is due to the consideration of feedback  
555 processes among chemistry, aerosol, cloud, and radiation in the two-way coupled WRF-CMAQ  
556 simulation.

557 Figure 9 shows the difference plots of selected major meteorological variables including  
558 SWDOWN, T2, RH2, WS10, PBL height, and precipitation between two-way WRF-CMAQ and  
559 WRF-only. As shown, the incoming shortwave radiation is reduced by up to  $24.8 \text{ W m}^{-2}$  (13.6%)  
560 with a domain-average of  $13.0 \text{ W m}^{-2}$  (6%) due to the combined aerosol direct and indirect  
561 radiative effects over the domain. The reduction is predominant over the eastern U.S. where both  
562 aerosol loading and cloud cover are high and over the oceans where cloud cover is high. The  
563 magnitude of shortwave radiation reduction in this work is consistent with other studies. For  
564 example, Wang et al. (2015) found that the combined aerosol direct and indirect effects using the  
565 WRF/Chem model, which includes the sub-scale cloud forcing not treated in the current WRF-  
566 CMAQ model, may decrease the incoming shortwave radiation by  $16.0 \text{ W m}^{-2}$  in the summer



567 over the U.S. Hogrefe et al. (2015) reported the reduction of shortwave radiation may reach up to  
568  $20 \text{ W m}^{-2}$  over the eastern U.S. by only considering the aerosol direct effect using an older  
569 version of WRF-CMAQ v5.0.1. Xing et al. (2015b) showed that the aerosol direct forcing may  
570 cause the surface shortwave radiation to decrease by up to  $10 \text{ W m}^{-2}$  over the eastern U.S. over a  
571 decadal time period using WRF-CMAQ v5.0. The reduction of shortwave radiation further  
572 reduces the surface temperature by up to  $0.25 \text{ }^{\circ}\text{C}$  over the eastern U.S., which is much larger  
573 than the reduction of  $0.1 \text{ }^{\circ}\text{C}$  reported by Hogrefe et al. (2015), mainly due to the inclusion of  
574 aerosol indirect effects. However there are smaller reductions of T2 over the Pacific Ocean and  
575 even increases (by up to  $0.1 \text{ }^{\circ}\text{C}$ ) over large areas of Atlantic Ocean and Gulf of Mexico where  
576 much larger reductions of shortwave radiation occur. As pointed by Wang et al. (2015), due to  
577 the much larger heat capacity of ocean, the response of sea surface temperature is less sensitive  
578 to the change of shortwave radiation for ocean compared to the land. The large increase of  
579 incoming longwave radiation and latent heat (figures not shown) caused by the aerosol indirect  
580 effects and other complex feedback processes over the ocean compensates for the reduction of  
581 shortwave radiation, especially over the Atlantic Ocean and Gulf of Mexico, and thus leads to  
582 less reduction or even increases of T2. RH2 is found to mostly increase by 3.4% over the land  
583 caused by the decrease of temperature while decrease by 2.6% over the ocean caused by either  
584 the increase of temperature or large decrease of water vapor. Over the land, the decreases in solar  
585 radiation and T2 along with the latent heat (figure not shown) lead to a more stable PBL and thus  
586 suppress the wind (by reducing the wind speed as shown). Over the ocean, the changes lead to a  
587 more unstable PBL and thus enhance the wind over the ocean. The wind speed and PBL height  
588 are reduced by up to  $0.05 \text{ m s}^{-1}$  and 25 m, respectively, over the U.S. The aerosol feedbacks on  
589 precipitation are also mixed with relatively large decreases by up to  $0.4 \text{ mm day}^{-1}$  over the U.S.



590 and increases by up to  $0.4 \text{ mm day}^{-1}$  over oceans. The suppression of precipitation over the land  
591 is mainly due to the formation of more small sized CCNs caused by aerosol indirect effects and  
592 align well with areas with high aerosol loadings while the enhancement of precipitation,  
593 especially along coastlines and over oceans, might be associated with the larger CCN formation  
594 via more activated sea-salt particles as indicated by Zhang et al. (2010) and Wang et al. (2015).

#### 595 **4.2 Air Quality**

596 Figures 5 and 6 compare observations and simulations from two-way WRF-CMAQ and  
597 offline CMAQ for  $\text{O}_3$ ,  $\text{PM}_{2.5}$ , and  $\text{PM}_{2.5}$  constituents. Table 2 summarizes the statistics for all  
598 major chemical variables for the two simulations. As shown in Figure 5, two-way WRF-CMAQ  
599 shows better performance for both the monthly variation of  $\text{O}_3$  (throughout the whole year) over  
600 AQS sites and the diurnal pattern of  $\text{O}_3$  (especially during winter) over CASTNET sites due to  
601 better performance of T2 and radiation compared to offline WRF and CMAQ. As shown in  
602 Figure 6, two-way WRF-CMAQ shows similar spatial distribution of  $\text{PM}_{2.5}$  and better  
603 performance for  $\text{PM}_{2.5}$  for most of months over CSN sites and for cold seasons across  
604 IMPROVE sites compared to offline CMAQ. It also shows systematically better performance for  
605  $\text{SO}_4^{2-}$ ,  $\text{NO}_3^-$ ,  $\text{NH}_4^+$ , and TC with more data within 1:2 and closer to 1:1 ratio lines of scatter plots.  
606 Overall, as shown in Table 2, both simulations show generally good performance for all major  
607 chemical species except for  $\text{PM}_{10}$ . For example., the domain-average NMBs are 12.6% (AQS)  
608 and 1.5% (CASTNET) vs. 17.7% (AQS) and 7.7% (CASTNET) for  $\text{O}_3$  and -7.0% (CSN) and -  
609 13.7% (IMPROVE) vs. -3.4% (CSN) and -5.7% (IMPROVE) for  $\text{PM}_{2.5}$  for two-way WRF-  
610 CMAQ and offline-coupled CMAQ, respectively. The two-way WRF-CMAQ shows better  
611 domain-wide statistics in terms of both correlation and biases for many variables including  $\text{O}_3$ ,  
612  $\text{SO}_4^{2-}$ ,  $\text{NO}_3^-$ ,  $\text{NH}_4^+$ , and EC as well as TOR and column  $\text{NO}_2$ , apparently due to the treatment of



613 chemistry-meteorology feedbacks. Offline CMAQ performs better for total PM<sub>2.5</sub> especially in  
614 the western U.S. due to higher dust emissions from higher wind speed and higher SOA due to  
615 stronger radiation and higher temperature. However more robust comparisons are needed in the  
616 future with improved dust emissions and the use of FINN wildfire emissions.

617 Figure 10 shows the difference plots of selected chemical variables including CO, O<sub>3</sub>,  
618 NO<sub>x</sub>, volatile organic compounds (VOCs), SO<sub>4</sub><sup>2-</sup>, SOA, PM<sub>2.5</sub>, and PM<sub>10</sub> between two-way  
619 WRF-CMAQ and offline-coupled CMAQ. As shown, the CO mixing ratios decrease by up to  
620 79.2 ppb (27.8%) especially over the western U.S. with a domain-average reduction of 3.0 ppb  
621 (3.1%) due to reduced formation of CO from the oxidation of VOCs caused by reduced solar  
622 radiation as indicated by Zhang et al. (2017). Such reductions seem to dominate over the  
623 increases caused by reduced PBL height, especially in the western U.S. where PBL height  
624 reductions are minimum. The O<sub>3</sub> mixing ratios decrease by up to 5.2 ppb (16.2%) with domain-  
625 average of 1.7 ppb (4.2%) mainly due to the reduced solar radiation and T2. The change of O<sub>3</sub> is  
626 consistent with other studies such as Makar et al. (2015) and Wang et al. (2015) that also  
627 reported lower O<sub>3</sub> mixing ratios caused by aerosol direct and indirect effects. On the other hand,  
628 both NO<sub>x</sub> and VOC mixing ratios increase over the eastern U.S. while they decrease over the  
629 western U.S. The increase should be caused by the combination of the large reduction of PBL  
630 mixing and reduced solar radiation which reduces NO<sub>2</sub> photolysis and VOC oxidation to SOA.  
631 For aerosol species, SO<sub>4</sub><sup>2-</sup> concentrations increase by up to 0.38 μg m<sup>-3</sup> (26.6%) especially over  
632 the eastern U.S. In fact, the reduction of O<sub>3</sub> mixing ratios due to aerosol effects is expected to  
633 reduce SO<sub>4</sub><sup>2-</sup> production via the gas-phase oxidation pathway due to the influence of O<sub>3</sub> on OH,  
634 but increase SO<sub>4</sub><sup>2-</sup> production via the aqueous-phase chemistry pathway due to more clouds in  
635 the two-way WRF-CMAQ simulation. Thus, the net increase of SO<sub>4</sub><sup>2-</sup> is more dominated by the



636 aqueous-phase chemistry instead of the gas-phase oxidation. This net increase of  $\text{SO}_4^{2-}$ , in turn,  
637 leads to an increase of  $\text{NH}_4^+$  and decrease of  $\text{NO}_3^-$  (figures not shown) through aerosol  
638 thermodynamic equilibrium. SOA concentrations decrease by up to  $0.34 \mu\text{g m}^{-3}$  (41.6%)  
639 especially over the eastern U.S. due to the large reduction of oxidants.  $\text{PM}_{2.5}$  concentrations also  
640 decrease by up to  $5.2 \mu\text{g m}^{-3}$  (49.1%) with a domain-average of  $0.34 \mu\text{g m}^{-3}$  (8.6%), and  $\text{PM}_{10}$   
641 concentrations decrease by up to  $19.3 \mu\text{g m}^{-3}$  (64.8%) with a domain-average of  $1.1 \mu\text{g m}^{-3}$   
642 (11.1%). The reductions are more apparent over the western U.S. than the eastern U.S. partially  
643 due to the compensation of the increase of  $\text{SO}_4^{2-}$  and  $\text{NH}_4^+$  and decrease of other secondary  
644 aerosols over the eastern U.S., as well as the relatively large reduction of dust concentrations  
645 over the western U.S. caused by reduced wind speed.

## 646 5. Summary and conclusion

647 In this study, two sets of long-term simulations for 2008-2012 using the two-way coupled  
648 WRF-CMAQ and offline coupled WRF and CMAQ, respectively, are conducted, evaluated, and  
649 compared to investigate the performance improvements due to chemistry-meteorology feedbacks  
650 and impacts of those feedbacks on the regional air quality in the U.S. First, the two-way coupled  
651 WRF-CMAQ simulation with both aerosol direct and indirect radiative forcing is  
652 comprehensively evaluated. The results show that WRF-CMAQ performs well for major surface  
653 meteorological variables such as temperature at 2 m, relative humidity at 2 m, wind speed at 10  
654 m, and precipitation with domain-average MBs of  $0.1 \text{ }^\circ\text{C}$ , 2.2 %,  $0.44 \text{ m s}^{-1}$ , and  $0.14\text{-}0.28 \text{ mm}$   
655  $\text{day}^{-1}$  (except for  $0.71 \text{ mm day}^{-1}$  against NCDC), respectively. The overall small warm bias  
656 compared to other studies is most likely associated with the soil moisture nudging technique used  
657 in the PX land surface scheme. The relatively large positive biases for precipitation are found to  
658 be more apparent when observed precipitation is low (dominated more by the non-convective



659 precipitation) and are thus believed to be more associated with uncertainties in the Morrison  
660 microphysics scheme. The long-term simulation also shows generally good performance for  
661 major radiation and cloud radiative variables. Relatively large model biases still exist for cloud  
662 variables such as CDNC, COT, and CWP, indicating that the processes associated with aerosol  
663 indirect effects are still not well understood and an accurate simulation of those effects is still  
664 challenging using state-of-the-science models.

665 Two-way WRF-CMAQ also shows generally good or acceptable performance for max 8-  
666 h O<sub>3</sub>, PM<sub>2.5</sub> and PM<sub>2.5</sub> constituents, with NMBs generally within ±15% for O<sub>3</sub> and ±30% for  
667 PM<sub>2.5</sub> species. For example, the domain-average NMBs are 12.6 % and 1.5 % for max 8-h O<sub>3</sub>  
668 against AQS and CASTNET and -7.0 % and -13.7 % for PM<sub>2.5</sub> against CSN and IMPROVE,  
669 respectively. O<sub>3</sub> mixing ratios are overpredicted for most months, especially in the winter, in part  
670 due to the larger overprediction of T2 during the cold season. The overall model biases are small  
671 for PM<sub>2.5</sub> due to the compensation of relatively large underpredictions of SO<sub>4</sub><sup>2-</sup> and OC,  
672 especially in the warm season, and overprediction of NO<sub>3</sub><sup>-</sup> in the cold season. In addition to  
673 biases inherited from the meteorology, the model performance for chemistry also suffers from  
674 uncertainties associated with emissions, the use of a coarse spatial resolution, and representation  
675 of aerosol formation pathways in the model. For example, the relatively large biases for EC  
676 might be associated with poorly allocated anthropogenic/wildfire emissions and those for OC  
677 might be due to underestimation of SOA formation in version 5.0.2 of CMAQ. WRF-CMAQ  
678 also predicts the column abundances of chemical species well and the relatively large model  
679 biases for CO are found to be associated with an underestimation of BCONs. The model better  
680 reproduces the observed number of exceedance days for O<sub>3</sub> than PM<sub>2.5</sub> mainly due to better  
681 performance for O<sub>3</sub> than PM<sub>2.5</sub> concentrations.



682           The performance comparison between two-way WRF-CMAQ and WRF-only simulations  
683 shows that two-way WRF-CMAQ model performs better for major surface meteorological,  
684 radiation, and cloud radiative variables due to the consideration of chemistry-meteorology  
685 feedbacks associated with aerosol direct and indirect forcing. The feedbacks are found to reduce  
686 the 5-year average SWDOWN by up to 24.8 W m<sup>-2</sup>, T2 by up to 0.25 °C, PBL height by up to 25  
687 m, wind speed by up to 0.05 m s<sup>-1</sup>, and precipitation by up to 0.4 mm day<sup>-1</sup> over the CONUS,  
688 which in turn affect the air quality significantly. As a result of feedbacks, two-way WRF-CMAQ  
689 outperforms offline CMAQ for O<sub>3</sub>, SO<sub>4</sub><sup>2-</sup>, NO<sub>3</sub><sup>-</sup>, NH<sub>4</sub><sup>+</sup>, and EC as well as TOR and column NO<sub>2</sub>  
690 in terms of both spatiotemporal variations and domain-average statistics due to better  
691 meteorology performance for variables such as T2, WS10, radiation, and precipitation. Despite  
692 these improvements, the offline CMAQ performs better for total PM<sub>2.5</sub> in terms of domain-  
693 average statistics, which could be partially caused by the compensation of larger under- and  
694 over-predictions of PM<sub>2.5</sub> constituents. More robust comparison for PM<sub>2.5</sub> should be performed  
695 with improved dust and wildfire emissions in future work. Chemistry-meteorology feedbacks are  
696 found to play important roles in affecting U.S. air quality by reducing domain-wide 5-year  
697 average surface CO by 3.0 ppb (3.1%) and up to 79.2 ppb (27.8%), O<sub>3</sub> by 1.7 ppb (4.1%) and up  
698 to 5.2 ppb (16.2%), PM<sub>2.5</sub> by 0.34 μg m<sup>-3</sup> (8.6%) and up to 5.2 μg m<sup>-3</sup> (49.1%), and PM<sub>10</sub> by 1.1  
699 μg m<sup>-3</sup> (11.1%) and up to 19.3 μg m<sup>-3</sup> (64.8%) mainly due to reduction of radiation, temperature,  
700 and wind speed.

701           In summary, the two-way coupled WRF-CMAQ modeling in this study shows generally  
702 satisfactory and consistent performance for the long-term prediction of regional meteorology and  
703 air quality when compared to other studies in the literature. Possible causes for the  
704 meteorological and chemical biases that were identified through this work can provide valuable



705 information for future model development to improve the two-way coupled WRF-CMAQ model  
706 and those biases should also be considered when making future climate/air quality projections.  
707 Non-negligible model improvements for many major meteorological and chemical variables  
708 compared to the traditional application of offline coupled WRF and CMAQ suggest the  
709 importance of chemistry-meteorology feedbacks, especially aerosol direct and indirect effects.  
710 The feedbacks should be considered along with other factors in developing future model  
711 applications to inform policy making.

#### 712 **Code Availability**

713 The modeling system used in this study is based on the 2-way coupled WRF-CMAQ model  
714 derived from WRF v3.4 and CMAQ v5.0.2. Relevant code for CMAQ v5.0.2, its coupling to  
715 WRF and aerosol direct feedbacks are publicly available from: doi:10.5281/zenodo.1079898.  
716 WRF v3.4 code can be downloaded from  
717 [http://www2.mmm.ucar.edu/wrf/users/download/get\\_source.html](http://www2.mmm.ucar.edu/wrf/users/download/get_source.html). The version of the coupled  
718 WRF-CMAQ model with the additional indirect aerosol forcing approach of Yu et al. (2014) can  
719 be downloaded from the following website: <https://person.zju.edu.cn/shaocaiyu#674502>.

#### 720 **Author contribution**

721 YZ and KW designed the study and all the simulations. SY developed the two-way coupled  
722 WRF-CMAQ code. KW conducted all the simulations and performed the analyses. KW prepared  
723 the manuscript with contributions from all co-authors.

#### 724 **Competing interests**

725 The authors declare that they have no conflict of interest.



726 **Acknowledgements**

727 This work was developed at North Carolina State University and Northeastern University under  
728 Assistance Agreement No. RD835871 awarded by the U.S. Environmental Protection Agency to  
729 Yale University. The views expressed in this manuscript are those of the authors alone and do  
730 not necessarily reflect the views and policies of the U.S. Environmental Protection Agency. EPA  
731 does not endorse any products or commercial services mentioned in this publication. High  
732 performance computing was support from Yellowstone (ark:/85065/d7wd3xhc) provided by  
733 NCAR's CISL, sponsored by the NSF and the Stampede XSEDE high-performance computing  
734 support under the NSF ACI-1053575. The work of S. Yu is supported by the Department of  
735 Science and Technology of China (No. 2016YFC0202702, 2018YFC0213506 and  
736 2018YFC0213503), National Research Program for Key Issues in Air Pollution Control in China  
737 (No. DQGG0107) and National Natural Science Foundation of China (No. 21577126 and  
738 41561144004). The authors gratefully acknowledge the availability of CERES, GPCP, MODIS,  
739 MOPITT, NCDC, OMI, PRISM, SCHIAMACHY, and TMPA data. The authors thank Dr. Ralf  
740 Bennartz from Vanderbilt University for providing the CDNC data. The authors also would like  
741 to thank Drs. Jerry Herwehe and Shannon Koplitz from the U.S. EPA for their constructive and  
742 very helpful comments.

743 **References**

- 744 Abdul-Razzak, H. and Ghan, S. J.: A parameterization of aerosol activation 2. Multiple aerosol  
745 types, *J. Geophys. Res.*, 105 (D3), 6837-6844, 2000.
- 746 Alapaty, K., Herwehe, J. A., Otte, T. L., Nolte, C. G., Bullock, O. R., Mallard, M. S., Kain, J. S.,  
747 and Dudhia, J.: Introducing subgrid-scale cloud feedbacks to radiation for regional  
748 meteorological and climate modeling, *Geophys. Res. Lett.*, 39, L24809,  
749 <https://doi.org/10.1029/2012GL054031>, 2012.



- 750 Allen, D. J., Pickering, K. E., Pinder, R. W., Henderson, B. H., Appel, K. W., and Prados, A.:  
751 Impact of lightning-NO on eastern United States photochemistry during the summer of 2006 as  
752 determined using the CMAQ model, *Atmos. Chem. Phys.*, 12, 1737-  
753 1758, <https://doi.org/10.5194/acp-12-1737-2012>, 2012.
- 754 Appel, K. W., Gilliland, A. B., Sarwar, G., and Gilliam, R. C.: Evaluation of the Community  
755 Multiscale Air Quality (CMAQ) model version 4.5: Sensitivities impacting model performance:  
756 Part I, Ozone, *Atmos. Environ.*, 41, 9603-9615, 2007.
- 757 Appel, K. W., Pouliot, G. A., Simon, H., Sarwar, G., Pye, H. O. T., Napelenok, S. L., Akhtar, F.,  
758 and Roselle, S. J.: Evaluation of dust and trace metal estimates from the Community Multiscale  
759 Air Quality (CMAQ) model version 5.0, *Geosci. Model Dev.*, 6, 883–899,  
760 <https://doi.org/10.5194/gmd-6-883-2013>, 2013.
- 761 Appel, K. W., Napelenok, S. L., Foley, K. M., Pye, H. O. T., Hogrefe, C., Luecken, D. J., Bash,  
762 J. O., Roselle, S. J., Pleim, J. E., Foroutan, H., Hutzell, W. T., Pouliot, G. A., Sarwar, G., Fahey,  
763 K. M., Gantt, B., Gilliam, R. C., Heath, N. K., Kang, D., Mathur, R., Schwede, D. B., Spero, T.  
764 L., Wong, D. C., and Young, J. O.: Description and evaluation of the Community Multiscale Air  
765 Quality (CMAQ) modeling system version 5.1, *Geosci. Model Dev.*, 10, 1703–1732,  
766 <https://doi.org/10.5194/gmd-10-1703-2017>, 2017.
- 767 Baklanov, A., Schlünzen, K. H., Suppan, P., Baldasano, J., Brunner, D., Aksoyoglu, S.,  
768 Carmichael, G., Douros, J., Flemming, J., Forkel, R., Galmarini, S., Gauss, M., Grell, G., Hirtl,  
769 M., Joffre, S., Jorba, O., Kaas, E., Kaasik, M., Kallos, G., Kong, X., Korsholm, U., Kurganski,  
770 A., Kushta, J., Lohmann, U., Mahura, A., Manders-Groot, A., Maurizi, A., Moussiopoulos, N.,  
771 Rao, S. T., Savage, N., Seigneur, C., Sokhi, R. S., Solazzo, E., Solomos, S., Sørensen, B.,  
772 Tsegas, G., Vignati, E., Vogel, B., and Zhang, Y.: Online coupled regional meteorology-  
773 chemistry models in Europe: Current status and prospects, *Atmos. Chem. Phys.*, 14, 317-398,  
774 doi:10.5194/acp-14-317-2014, 2014.
- 775 Bennartz, R.: Global assessment of marine boundary layer cloud droplet number concentration  
776 from satellite, *J. Geophys. Res.*, 112, D02201, <http://dx.doi.org/10.1029/2006JD007547>, 2007.
- 777 Boersma, K. F., Eskes, H. J., and Brinksma, E. J.: Error analysis for tropospheric NO<sub>2</sub> retrieval  
778 from space, *J. Geophys. Res.*, 109, D04311, doi:10.1029/2003JD003962, 2004.
- 779 Brunner, D., Savage, N., Jorba, O., Eder, B., Giordano, L., Badia, A., Balzarini, A., Baro, R.,  
780 Bianconi, R., Chemel, C., Curci, G., Forkel, R., Jimenez-Guerrero, P., Hirtl, M., Hodzic, A.,  
781 Hozak, L., Im, U., Knote, C., Makar, P., Manders-Groot, A., van Meijgaard, E., Neal, L., Perez,  
782 J. L., Pirovano, G., San Jose, R., Schroder, W., Sokhi, R. S., Syrakov, D., Torian, A., Tuccella,  
783 P., Werhahn, J., Wolke, R., Yahya, K., Zabkar, R., Zhang, Y., Hogrefe, C., and Galmarini, S.:  
784 Comparative analysis of meteorological performance of coupled chemistry-meteorology models  
785 in the context of AQMEII phase 2, *Atmos. Environ.*, 115, 470–498,  
786 doi:10.1016/j.atmosenv.2014.12.032, 2015.
- 787 Byun, D. W. and Schere K. L.: Review equations, computational algorithms, and other  
788 components of the Models-3 Community Multi-Scale Air Quality (CMAQ) modeling system,  
789 *Applied Mechanics Reviews*, 59(2), 51-77, doi:10.1115/1.2128636, 2006.



- 790 Choi, M.W., Lee, J. H., Woo, J. W., Kim, C. H., and Lee, S. H.: Comparison of PM<sub>2.5</sub> chemical  
791 components over East Asia simulated by the WRF-Chem and WRF/CMAQ models: On the  
792 models' prediction inconsistency, *Atmosphere*, 10, 618, 2019.
- 793 Cohen, A. E., Cavallo, S. M., Coniglio, M. C., and Brooks, H. E.: A review of planetary  
794 boundary layer parameterization schemes and their sensitivity in simulating southeastern U.S.  
795 cold season severe weather environments, *Weather and Forecasting*,  
796 <https://doi.org/10.1175/WAF-D-14-00105.1>, 2015.
- 797 Dong, X., Fu, J. S., Huang, K., Tong, D., and Zhuang, G.: Model development of dust emission  
798 and heterogeneous chemistry within the Community Multiscale Air Quality modeling system  
799 and its application over East Asia, *Atmos. Chem. Phys.*, 16, 8157–8180,  
800 <https://doi.org/10.5194/acp-16-8157-2016>, 2016.
- 801 Eder, B. and Yu, S.: A performance evaluation of the 2004 release of Models-3 CMAQ, *Atmos.*  
802 *Environ.*, 40(26):4811-4824, 2006.
- 803 Emery, C., Liu, Z., Russell, A. G., Odman, M. T., Yarwood, G., and Kumar, N.:  
804 Recommendations on statistics and benchmarks to assess photochemical model performance, *J.*  
805 *Air Waste Manage. Assoc.*, 67:5, 582-598, doi:10.1080/10962247.2016.1265027, 2017.
- 806 Emmons, L. K., Edwards, D. P., Deeter, M. N., Gille, J. C., Campos, T., Nédélec, P., Novelli, P.,  
807 and Sachse, G.: Measurements of Pollution In The Troposphere (MOPITT) validation through  
808 2006, *Atmos. Chem. Phys.*, 9, 1795–1803, <https://doi.org/10.5194/acp-9-1795-2009>, 2009.
- 809 Foroutan, H., Young, J., Napelenok, S., Ran, L., Appel, K. W., Gilliam, R. C., and Pleim, J. E.:  
810 Development and evaluation of a physics-based windblown dust emission scheme implemented  
811 in the CMAQ modeling system, *J. Adv. Model. Earth Syst.*, 9, 585–608,  
812 doi:10.1002/2016MS000823, 2017.
- 813 Gan, C.-M., Pleim, J., Mathur, R., Hogrefe, C., Long, C. N., Xing, J., Wong, D., Gilliam, R., and  
814 Wei, C.: Assessment of long-term WRF–CMAQ simulations for understanding direct aerosol  
815 effects on radiation "brightening" in the United States, *Atmos. Chem. Phys.*, 15, 12193–12209,  
816 <https://doi.org/10.5194/acp-15-12193-2015>, 2015a.
- 817 Gan, C.-M., Binkowski, F., Pleim, J., Xing, J., Wong, D., Mathur, R., and Gilliam, R.:  
818 Assessment of the aerosol optics component of the coupled WRF–CMAQ model using CARES  
819 field campaign data and a single column model, *Atmos. Environ.*, 115, 670-682, 2015b.
- 820 Gantt, B., He, J., Zhang, X., Zhang, Y., and Nenes, A.: Incorporation of advanced aerosol  
821 activation treatments into CESM/CAM5: model evaluation and impacts on aerosol indirect  
822 effects, *Atmos. Chem. Phys.*, 14, 7485–7497, <https://doi.org/10.5194/acp-14-7485-2014>, 2014.
- 823 Gantt, B., Sarwar, G., Xing, J., Simon, H., Schwede, D., Hutzell, W. T., Mathur, R., and Saiz-  
824 Lopez, A.: The impact of iodide-mediated ozone deposition and halogen chemistry on surface  
825 ozone concentrations across the continental United States, *Environ. Sci. Technol.*, 51 (3), 1458-  
826 1466, 2017.



- 827 Ghan, S. J., Laulainen, N. S., Easter, R. C., Wagener, R., Nemesure, S., Chapman, E. G., Zhang,  
828 Y., and Leung, L. R.: Evaluation of aerosol direct radiative forcing in MIRAGE, *J. Geophys.*  
829 *Res.*, 106, 5295–5316, 2001.
- 830 Glotfelty, T., He, J., and Zhang, Y.: Impact of future climate policy scenarios on air quality and  
831 aerosol-cloud interactions using an advanced version of CESM/CAM5: Part I. model evaluation  
832 for the current decadal simulations, *Atmos. Environ.*, 152, 222-239, 2017.
- 833 Grell, G. A., Peckham, S. E., Schmitz, R., McKenn, S. A., Frost, G., Skamarock, W. C., and  
834 Eder, B.: Fully Coupled “Online” chemistry within the WRF Model, *Atmos. Environ.*, 39, 6957–  
835 6975, 2005.
- 836 Grell, G. A. and Baklanov, A.: Integrated modelling for forecasting weather and air quality: A  
837 call for fully coupled approaches, *Atmos. Environ.*, 45, 38, 6845–6851, 2011.
- 838 He, J. and Zhang, Y.: Improvement and further development in CESM/CAM5: Gasphase  
839 chemistry and inorganic aerosol treatments, *Atmos. Chem. Phys.*, 14, 9171-9200,  
840 <http://dx.doi.org/10.5194/acp-14-9171-2014>, 2014.
- 841 Heald, C. L., Jacob, D. J., Fiore, A. M., Emmons, L. K., Gille, J. C., Deeter, M. N., Warner, J.,  
842 Edwards, D. P., Crawford, J. H., Hamlin, A. J., Sachse, G. W., Browell, E. V., Avery, M. A.,  
843 Vay, S. A., Westberg, D. J., Blake, D. R., Singh, H. B., Sandholm, S. T., Talbot, R. W., and  
844 Fuelberg, H. E.: Asian outflow and trans-Pacific transport of carbon monoxide and ozone  
845 pollution: An integrated satellite, aircraft, and model perspective, *J. Geophys. Res.*, 108(D24),  
846 4804, doi:10.1029/2003JD003507, 2003.
- 847 Herwehe, J. A., Otte, T. L., Mathur, R., and Rao, S. T.: Diagnostic analysis of ozone  
848 concentrations simulated by two regional-scale air quality models, *Atmos. Environ.*, 45, 5957–  
849 5969, 2011.
- 850 Hogrefe, C., Pouliot, G., Wong, D., Torian, A., Roselle, S., Pleim, J., and Mathur, R.: Annual  
851 application and evaluation of the online coupled WRF–CMAQ system over North America  
852 under AQMEII phase 2, *Atmos. Environ.*, 115, 683-694, 2015.
- 853 Hong, C., Zhang, Q., Zhang, Y., Tang, Y., Tong, D., and He, K.: Multi-year downscaling  
854 application of two-way coupled WRF v3.4 and CMAQ v5.0.2 over east Asia for regional climate  
855 and air quality modeling: model evaluation and aerosol direct effects, *Geosci. Model Dev.*, 10,  
856 2447–2470, <https://doi.org/10.5194/gmd-10-2447-2017>, 2017.
- 857 Hong, C.-P., Zhang, Q., Zhang, Y., Davis, S. J., Zhang, X., Tong, D., Guan, D., Liu, Z., and He,  
858 K.-B.: Weakened aerosol radiative effects may mitigate the climate penalty on Chinese air  
859 quality, *Nature Climate Change*, in press, 2020.
- 860 Iacono, M. J., Delamere, J. S., Mlawer, E. J., Shephard, M. W., Clough, S. A., and Collins, W.  
861 D.: Radiative forcing by long-lived greenhouse gases: Calculations with the AER radiative  
862 transfer models, *J. Geophys. Res. Atmos.*, 113, D13103, <https://doi.org/10.1029/2008JD009944>,  
863 2008.



- 864 IPCC: Global warming of 1.5°C, An IPCC Special Report on the impacts of global warming of  
865 1.5°C above pre-industrial levels and related global greenhouse gas emission pathways, in the  
866 context of strengthening the global response to the threat of climate change, sustainable  
867 development, and efforts to eradicate poverty edited by Masson-Delmotte, V., Zhai, P., Pörtner,  
868 H. O., Roberts, D., Skea, J., Shukla, P. R., Pirani, A., Moufouma-Okia, W., Péan, C., Pidcock,  
869 R., Connors, S., Matthews, J. B. R., Chen, Y., Zhou, X., Gomis, M. I., Lonnoy, E., Maycock, T.,  
870 Tignor, M., and Waterfield, T., 2018.
- 871 Jacobson, M. Z., Lu, R., Turco, R. P., and Toon, O. B.: Development and application of a new  
872 air pollution modeling system. Part I: Gas-phase simulations, *Atmos. Environ.*, 30B, 1939–1963,  
873 1996.
- 874 Jacobson, M. Z.: GATOR-GCMM: A global- through urban-scale air pollution and weather  
875 forecast model 1. Model design and treatment of subgrid soil, vegetation, roads, rooftops, water,  
876 sea, ice, and snow, *J. Geophys. Res.*, 106, 5385–5401, 2001.
- 877 Jung, J., Souri, A. H., Wong, D. C., Lee, S., Jeon, W., Kim, J., and Choi, Y.: The impact of the  
878 direct effect of aerosols on meteorology and air quality using aerosol optical depth assimilation  
879 during the KORUS - AQ campaign, *J. Geophys. Res. Atmos.*, 124, 8303–8319,  
880 <https://doi.org/10.1029/2019JD030641>, 2019.
- 881 Kain, J. S.: The Kain-Fritsch convective parameterization: An update, *J. Appl. Meteorol.*, 43,  
882 170–181, [https://doi.org/10.1175/1520-0450\(2004\)043<0170:TKCPAU>2.0.CO;2](https://doi.org/10.1175/1520-0450(2004)043<0170:TKCPAU>2.0.CO;2), 2004.
- 883 Karydis, V. A., Tsimpidi, A. P., and Pandis, S. N.: Evaluation of a three-dimensional chemical  
884 transport model (PMCAMx) in the eastern United States for all four seasons, *J. Geophys. Res.*,  
885 112, D14211, doi:10.1029/2006JD007890, 2007.
- 886 Kaufman, Y. J., Smirnov, A., Holben, B., and Dubovik, O.: Baseline maritime aerosol  
887 methodology to derive the optical thickness and scattering properties, *Geophys. Res. Lett.*, 28,  
888 3251, doi:10.1029/2001GL013312, 2001.
- 889 Kelly, J., Koplitz, S., Baker, K., Holder, A., Pye, H., Murphy, B., Bash, J., Henderson, B.,  
890 Possiel, N., Simon, H., Eyth, A., Jang, C., Phillips, S., and Timin, B.: Assessing PM<sub>2.5</sub> model  
891 performance for the conterminous U.S. with comparison to model performance statistics from  
892 2007–2015, *Atmos. Environ.*, 214, <https://doi.org/10.1016/j.atmosenv.2019.116872>, 2019.
- 893 Kukkonen, J., Olsson, T., Schultz, D. M., Baklanov, A., Klein, T., Miranda, A. I., Monteiro, A.,  
894 Hirtl, M., Tarvainen, V., Boy, M., Peuch, V.-H., Poupkou, A., Kioutsioukis, I., Finardi, S.,  
895 Sofiev, M., Sokhi, R., Lehtinen, K. E. J., Karatzas, K., San José, R., Astitha, M., Kallos, G.,  
896 Schaap, M., Reimer, E., Jakobs, H., and Eben, K.: A review of operational, regional-scale,  
897 chemical weather forecasting models in Europe, *Atmos. Chem. Phys.*, 12, 1–87,  
898 doi:10.5194/acp-12-1-2012, 2012.
- 899 Li, P., Wang, L., Guo, P., Yu, S., Mehmood, K., Wang, S., Liu, W., Seinfeld, J. H., Zhang, Y.,  
900 Wong, D., Alapaty, K., Pleim, J., and Mathur, R.: High reduction of ozone and particulate matter  
901 during the 2016 G-20 summit in Hangzhou by forced emission controls of industry and traffic,  
902 *Environ. Chem. Lett.*, 15:709–715, doi:10.1007/s10311-017-0642-2, 2017.



- 903 Lin, M., Holloway, T., Carmichael, G. R., and Fiore, A. M.: Quantifying pollution inflow and  
904 outflow over East Asia in spring with regional and global models, *Atmos. Chem. Phys.*, 10,  
905 4221–4239, <https://doi.org/10.5194/acp-10-4221-2010>, 2010.
- 906 Liu, X.-H., Zhang, Y., Xing, J., Zhang, Q., Wang, K., Streets, D. G., Jang, C. J., Wang, W.-X.,  
907 and Hao, J. M.: Understanding of regional air pollution over China using CMAQ:- Part II.  
908 Process analysis and ozone sensitivity to precursor emissions, *Atmos. Environ.*, 44(20), 3719-  
909 3727, 2010.
- 910 Lorente, A., Folkert Boersma, K., Yu, H., Dörner, S., Hilboll, A., Richter, A., Liu, M., Lamsal,  
911 L. N., Barkley, M., De Smedt, I., Van Roozendael, M., Wang, Y., Wagner, T., Beirle, S., Lin, J.-  
912 T., Krotkov, N., Stammes, P., Wang, P., Eskes, H. J., and Krol, M.: Structural uncertainty in air  
913 mass factor calculation for NO<sub>2</sub> and HCHO satellite retrievals, *Atmos. Meas. Tech.*, 10, 759–  
914 782, <https://doi.org/10.5194/amt-10-759-2017>, 2017.
- 915 Ma, P.-L., Rasch, P. J., Fast, J. D., Easter, R. C., Gustafson Jr., W. I., Liu, X., Ghan, S. J., and  
916 Singh, B.: Assessing the CAM5 physics suite in the WRF-Chem model: implementation,  
917 resolution sensitivity, and a first evaluation for a regional case study, *Geosci. Model Dev.*, 7,  
918 755–778, <https://doi.org/10.5194/gmd-7-755-2014>, 2014.
- 919 Makar, P., A., Gong, W., Hogrefe, C., Zhang, Y., Curci, G., Žabkar, R., Milbrandt, J., Im, U.,  
920 Balzarini, A., Baró, R., Bianconi, R., Cheung, P., Forkel, R., Gravel, S., Hirtl, M., Honzak, L.,  
921 Hou, A., Jiménez-Guerrero, P., Langer, M., Moran, M. B., Pabla, B., Pérez, J. L., Pirovano, G.,  
922 San José, R., Tuccella, P., Werhahn, J., Zhang, J., and Galmarini, S.: Feedbacks between air  
923 pollution and weather, Part 2: Effects on chemistry, *Atmos. Environ.*, 115, 499-526, 2015.
- 924 Mathur, R., Xiu, A., Coats, C., Alapaty, K., Shankar, U., and Hanna, A.: Development of an air  
925 quality modeling system with integrated meteorology, chemistry, and emissions, *Proc.*  
926 *Measurement of Toxic and Related Air Pollutants*, AWMA, Cary, NC, September, 1998.
- 927 Mathur, R., Xing, J., Gilliam, R., Sarwar, G., Hogrefe, C., Pleim, J., Pouliot, G., Roselle, S.,  
928 Spero, T. L., Wong, D. C., and Young, J.: Extending the Community Multiscale Air Quality  
929 (CMAQ) modeling system to hemispheric scales: overview of process considerations and initial  
930 applications, *Atmos. Chem. Phys.*, 17, 12449-12474, 2017.
- 931 Matsui, H., Koike, M., Kondo, Y., Takegawa, N., Kita, K., Miyazaki, Y., Hu, M., Chang, S.-Y.,  
932 Blake, D. R., Fast, J. D., Zaveri, R. A., Streets, D. G., Zhang, Q. and Zhu, T.: Spatial and  
933 temporal variations of aerosols around Beijing in summer 2006: Model evaluation and source  
934 apportionment, *J. Geophys. Res.*, 114, D00G13, doi:10.1029/2008JD010906, 2009.
- 935 Mebust, M. R., Eder, B. K., Binkowski, F. S., and Roselle, S. J.: Models-3 Community  
936 Multiscale Air Quality (CMAQ) model aerosol component: 2. Model evaluation, *J. Geophys.*  
937 *Res.*, 108(D6), 4184, doi:10.1029/2001JD001410, 2003.
- 938 Mehmood, K., Wu, Y., Wang, L., Yu, S., Li, P., Chen, X., Li, Z., Zhang, Y., Li, M., Liu, W.,  
939 Wang, Y., Liu, Z., Zhu, Y., Rosenfeld, D., and Seinfeld, J. H.: Relative effects of open biomass  
940 burning and open crop straw burning on haze formation over central and eastern China:  
941 modeling study driven by constrained emissions, *Atmos. Chem. Phys.*, 20, 2419–2443,  
942 <https://doi.org/10.5194/acp-20-2419-2020>, 2020.



- 943 Morrison, H., Thompson, G., and Tatarskii, V.: Impact of cloud microphysics on the  
944 development of trailing stratiform precipitation in a simulated squall line: Comparison of one-  
945 and two-moment schemes, *Mon. Weather Rev.*, 137, 991–1007,  
946 <https://doi.org/10.1175/2008MWR2556.1>, 2009.
- 947 Penrod, A., Zhang, Y., Wang, K., Wu, S.-Y., and Leung, R. L.: Impacts of future climate and  
948 emission changes on US air quality, *Atmos. Environ.*, 89, 533–547,  
949 doi:10.1016/j.atmosenv.2014.01.001, 2014.
- 950 Pleim, J. E.: A combined local and nonlocal closure model for the atmospheric boundary layer.  
951 Part I: Model description and testing, *J. Appl. Meteorol. Clim.*,  
952 <https://doi.org/10.1175/JAM2539.1>, 2007.
- 953 Pleim, J., Young, J., Wong, D., Gilliam, R., Otte, T., and Mathur, R.: Two-way coupled  
954 meteorology and air quality modeling, in *Air Pollution Modeling and its Application*, edited by  
955 C. Borrego and A. I. Miranda, XIX, NATO Science for Peace and Security Series, Series C:  
956 Environmental Security, Springer, Dordrecht, 2008.
- 957 Pleim, J. E. and Gilliam, R.: An indirect data assimilation scheme for deep soil temperature in  
958 the Pleim–Xiu land surface model, *J. Appl. Meteorol. Clim.*, 48, 1362–1376, 2009.
- 959 Pye, H. O. T., Murphy, B. N., Xu, L., Ng, N. L., Carlton, A. G., Guo, H., Weber, R., Vasilakos,  
960 P., Appel, K. W., Budisulistiorini, S. H., Surratt, J. D., Nenes, A., Hu, W., Jimenez, J. L.,  
961 Isaacman-VanWertz, G., Misztal, P. K., and Goldstein, A. H.: On the implications of aerosol  
962 liquid water and phase separation for organic aerosol mass, *Atmos. Chem. Phys.*, 17, 343–369,  
963 doi:10.5194/acp-17-343-2017, 2017.
- 964 Pye, H. O. T., Nenes, A., Alexander, B., Ault, A. P., Barth, M. C., Clegg, S. L., Collett Jr., J. L.,  
965 Fahey, K. M., Hennigan, C. J., Herrmann, H., Kanakidou, M., Kelly, J. T., Ku, I.-T., McNeill, V.  
966 F., Riemer, N., Schaefer, T., Shi, G., Tilgner, A., Walker, J. T., Wang, T., Weber, R., Xing, J.,  
967 Zaveri, R. A., and Zuend, A.: The acidity of atmospheric particles and clouds, *Atmos. Chem.*  
968 *Phys.*, 20, 4809–4888, <https://doi.org/10.5194/acp-20-4809-2020>, 2020.
- 969 Remer, L. A., Kaufman, Y. J., Tanré, D., Mattoo, S., Chu, D. A., Martins, J. V., Li, R. R.,  
970 Ichoku, C., Levy, R. C., and Kleidman, R. G.: The MODIS aerosol algorithm, products, and  
971 validation, *J. Atmos. Sci.*, 62, 947–973, 2005.
- 972 Roy, B., Pouliot, G. A., Gilliland, A., Pierce, T., Howard, S., Bhave, P. V., and Benjey, W.:  
973 Refining fire emissions for air quality modeling with remotely sensed fire counts: A wildfire case  
974 study, *Atmos. Environ.*, 41(3), 655–665, doi:10.1016/j.atmosenv.2006.08.037, 2007.
- 975 San Joaquin Valley Air Pollution Control District: 2018 Plan for the 1997, 2006, and 2012 PM<sub>2.5</sub>  
976 Standards, November 15, 2018, <https://www.valleyair.org/pmplans>, 2018.
- 977 Sarwar, G., Luecken, D., Yarwood, G., Whitten, G. Z., and Carter, W. P. L.: Impact of an  
978 updated carbon bond mechanism on predictions from the CMAQ modeling system: Preliminary  
979 assessment, *J. Appl. Meteor. Clim.*, 47, 3e14, 2008.



- 980 Sarwar, G., Gantt, B., Schwede, D., Foley, K., Mathur, R., and Saiz-Lopez, A.: Impact of  
981 enhanced ozone deposition and halogen chemistry on tropospheric ozone over the Northern  
982 Hemisphere, *Environ. Sci. Technol.*, 49 (15), 9203-9211, 2015.
- 983 Scheffe, R. D., Strum, M., Phillips, S. B., Thurman, J., Eyth, A., Fudge, S., Morris, M., Palma,  
984 T., and Cook, R.: Hybrid modeling approach to estimate exposures of hazardous air pollutants  
985 (HAPs) for the National Air Toxics Assessment (NATA), *Environ. Sci. Technol.*, 2016, 50(22),  
986 12356–12364, doi:10.1021/acs.est.6b04752, 2016.
- 987 Schwede, D., Pouliot, G. A., and Pierce, T.: Changes to the biogenic emissions inventory system  
988 version 3 (BEIS3), in: *Proceedings of the 4th CMAS Models-3 Users' Conference*, Chapel Hill,  
989 NC, 26–28 September, 2005.
- 990 Sekiguchi, A., Shimadera, H., and Kondo, A.: Impact of aerosol direct effect on wintertime  
991 PM<sub>2.5</sub> simulated by an online coupled meteorology-air quality model over East Asia, *Aerosol.*  
992 *Air Qual. Res.*, 18, 1068–1079, 2018.
- 993 Solazzo, E., Hogrefe, C., Colette, A., Garcia-Vivanco, M., and Galmarini, S.: Advanced error  
994 diagnostics of the CMAQ and Chimere modelling systems within the AQMEI3 model  
995 evaluation framework, *Atmos. Chem. Phys.*, 17, 10435-10465, 2017.
- 996 U.S. EPA: Policy assessment for the review of the National Ambient Air Quality Standards for  
997 particulate matter, EPA-452/R-20-002, January 2020,  
998 [https://www.epa.gov/sites/production/files/2020-](https://www.epa.gov/sites/production/files/2020-01/documents/final_policy_assessment_for_the_review_of_the_pm_naaqs_01-2020.pdf)  
999 [01/documents/final\\_policy\\_assessment\\_for\\_the\\_review\\_of\\_the\\_pm\\_naaqs\\_01-2020.pdf](https://www.epa.gov/sites/production/files/2020-01/documents/final_policy_assessment_for_the_review_of_the_pm_naaqs_01-2020.pdf), 2020.
- 1000 Vasilakos, P., Russell, A., Weber, R., and Nenes, A.: Understanding nitrate formation in a world  
1001 with less sulfate. *Atmos. Chem. Phys.* 18, 12765-12775, 2018.
- 1002 Wang, K. and Zhang, Y.: Application, evaluation, and process analysis of U.S. EPA's 2002  
1003 multiple-pollutant air quality modeling platform, *Atmospheric and Climate Sciences*, 2, 254-289,  
1004 2012.
- 1005 Wang, K. and Zhang, Y.: 3-D agricultural air quality modeling: Impacts of NH<sub>3</sub>/H<sub>2</sub>S gas-phase  
1006 reactions and bi-directional exchange of NH<sub>3</sub>, *Atmos. Environ.*, 98, 554-570, doi:  
1007 10.1016/j.atmosenv.2014.09.010, 2014.
- 1008 Wang, K., Zhang, Y., Jang, C., Phillips, S., and Wang, B.: Modeling intercontinental air  
1009 pollution transport over the trans-Pacific region in 2001 using the Community Multiscale Air  
1010 Quality modeling system, *J. Geophys. Res.*, 114, D04307, doi:10.1029/2008JD010807, 2009.
- 1011 Wang, K., Zhang, Y., Nenes, A., and Fountoukis, C.: Implementation of dust emission and  
1012 chemistry into the Community Multiscale Air Quality modeling system and initial application to  
1013 an Asian dust storm episode, *Atmos. Chem. Phys.*, 12, 10209–10237,  
1014 <https://doi.org/10.5194/acp-12-10209-2012>, 2012.
- 1015 Wang, J., Wang, S., Jiang, J., Ding, A., Zheng, M., Zhao, B., Wong, C.-D., Zhou, W., Zheng, G.,  
1016 Wang, L., Pleim, J., and Hao, J.: Impact of aerosol–meteorology interactions on fine particle



- 1017 pollution during China's severe haze episode in January 2013, *Environ. Res. Lett.*, 9,  
1018 doi:10.1088/1748-9326/9/9/094002, 2014.
- 1019 Wang, K., Zhang, Y., Yahya, K., Wu, S.-Y., and Grell, G.: Implementation and initial  
1020 application of new chemistry-aerosol options in WRF/Chem for simulating secondary organic  
1021 aerosols and aerosol indirect effects for regional air quality, *Atmos. Environ.*, 115, 716-732,  
1022 doi:10.1016/j.atmosenv.2014.12.007, 2015.
- 1023 West, J. J., Ansari, A. S., and Pandis, S. N.: Marginal PM<sub>2.5</sub>: Nonlinear aerosol mass response to  
1024 sulfate reductions in the Eastern United States, *J. Air Waste Manage. Assoc.*, 49, 1415-1424,  
1025 <https://doi.org/10.1080/10473289.1999.10463973>, 1999.
- 1026 Wiedinmyer, C., Quayle, B., Geron, C., Belote, A., McKenzie, D., Zhang, X., O'Neill, S., and  
1027 Wynne, K. K.: Estimating emissions from fires in North America for air quality modeling,  
1028 *Atmos. Environ.*, 40(19): 3419–32, doi:10.1016/j.atmosenv.2006.02.010, 2006.
- 1029 Wielicki, B. A., Barkstrom, B. R., Harrison, E. F., Lee III, R. B., Smith, G. L., and Cooper, J. E.:  
1030 Clouds and the Earth's Radiant Energy System (CERES): An earth observing system  
1031 experiment, *B. Am. Meteorol. Soc.*, 77, 853–868, 1996.
- 1032 Wilczak, J. M., Djalalova, I., McKeen, S., Bianco, L., Bao, J.-W., Grell, G., Peckham, S.,  
1033 Mathur, R., McQueen, J., and Lee, P.: Analysis of regional meteorology and surface ozone during  
1034 the TexAQS II field program and an evaluation of the NMM-CMAQ and WRF-Chem air quality  
1035 models, *J. Geophys. Res.*, 114, D00F14, 2009.
- 1036 Wong, D. C., Pleim, J., Mathur, R., Binkowski, F., Otte, T., Gilliam, R., Pouliot, G., Xiu, A.,  
1037 Young, J. O., and Kang, D.: WRF-CMAQ two-way coupled system with aerosol feedback:  
1038 Software development and preliminary results, *Geosci. Model Dev.*, 5, 299–312,  
1039 <https://doi.org/10.5194/gmd-5-299-2012>, 2012.
- 1040 Xing, J., Mathur, R., Pleim, J., Hogrefe, C., Gan, C.-M., Wong, D. C., Wei, C., and Wang, J.: Air  
1041 pollution and climate response to aerosol direct radiative effects: A modeling study of decadal  
1042 trends across the northern hemisphere, *J. Geophys. Res. Atmos.*, 120, 12,221–12,236,  
1043 doi:10.1002/2015JD023933, 2015a.
- 1044 Xing, J., Mathur, R., Pleim, J., Hogrefe, C., Gan, C.-M., Wong, D. C., and Wei, C.: Can a  
1045 coupled meteorology–chemistry model reproduce the historical trend in aerosol direct radiative  
1046 effects over the Northern Hemisphere?, *Atmos. Chem. Phys.*, 15, 9997–10018,  
1047 <https://doi.org/10.5194/acp-15-9997-2015>, 2015b.
- 1048 Xing, J., Wang, J., Mathur, R., Pleim, J., Wang, S., Hogrefe, C., Gan, C.-M., Wong, D., and Hao,  
1049 J.: Unexpected benefits of reducing aerosol cooling effects, *Environ. Sci. Technol.*, 50, 7527–  
1050 7534, <https://doi.org/10.1021/acs.est.6b00767>, 2016.
- 1051 Xing, J., Wang, J., Mathur, R., Wang, S., Sarwar, G., Pleim, J., Hogrefe, C., Zhang, Y., Jiang, J.,  
1052 Wong, D. C., and Hao, J.: Impacts of aerosol direct effects on tropospheric ozone through  
1053 changes in atmospheric dynamics and photolysis rates, *Atmos. Chem. Phys.*, 17, 9869–9883,  
1054 <https://doi.org/10.5194/acp-17-9869-2017>, 2017.



- 1055 Xiu, A. and Pleim, J. E.: Development of a land surface model. Part I: Application in a  
1056 mesoscale meteorological model, *J. Appl. Meteorol.*, 40, 192–209, <https://doi.org/10.1175/1520->  
1057 0450(2001)040<0192:doalsm>2.0.co;2, 2001.
- 1058 Yahya, K., Wang, K., Gudoshava, M., Glotfelty, T., and Zhang, Y.: Application of WRF/Chem  
1059 over North America under the AQMEII Phase 2. Part I. Comprehensive evaluation of 2006  
1060 simulation, *Atmos. Environ.*, 115, 733–755, doi:10.1016/j.atmosenv.2014.08.063, 2015a.
- 1061 Yahya, K., Wang, K., Zhang, Y., and Kleindienst, T. E.: Application of WRF/Chem over North  
1062 America under the AQMEII Phase 2 – Part 2: Evaluation of 2010 application and responses of  
1063 air quality and meteorology–chemistry interactions to changes in emissions and meteorology  
1064 from 2006 to 2010, *Geosci. Model Dev.*, 8, 2095–2117, <https://doi.org/10.5194/gmd-8-2095->  
1065 2015, 2015b.
- 1066 Yahya, K., Wang, K., Campbell, P., Glotfelty, T., He, J., and Zhang, Y.: Decadal evaluation of  
1067 regional climate, air quality, and their interactions over the continental US and their interactions  
1068 using WRF/Chem version 3.6.1, *Geosci. Model Dev.*, 9, 671–695, <https://doi.org/10.5194/gmd->  
1069 9-671-2016, 2016.
- 1070 Yarwood, G., Rao, S., Yocke, M., and Whitten, G. Z.: Final Report–Updates to the Carbon Bond  
1071 Chemical Mechanism: CB05, Rep.RT-04-00675, Yocke and Co., Novato, Calif., 246 pp., 2005.
- 1072 Yoo, J.-W., Jeon, W., Park, S.-Y., Park, C., Jung, J., Lee, S.-H., and Lee, H. W.: Investigating  
1073 the regional difference of aerosol feedback effects over South Korea using the WRF-CMAQ  
1074 two-way coupled modeling system, *Atmos. Environ.*, 218, 116968, 2019.
- 1075 Yu, S., Eder, B., Dennis, R., Chu, S., and Schwartz, S.: New unbiased symmetric metrics for  
1076 evaluation of air quality models, *Atmos. Sci. Lett.*, 7, 26–34, 2006.
- 1077 Yu, S. C., Mathur, R., Schere, K., Kang, D., Pleim, J., and Otte, T. L.: A detailed evaluation of  
1078 the Eta-CMAQ forecast model performance for O<sub>3</sub>, its related precursors, and meteorological  
1079 parameters during the 2004 ICARTT Study, *J. Geophys. Res.*, 112, D12S14,  
1080 doi:10.1029/2006JD007715, 2007.
- 1081 Yu, S. C., Mathur, R., Pleim, J., Wong, D., Carlton, A. G., Roselle, S., and Rao, S. T.:  
1082 Simulation of the indirect radiative forcing of climate due to aerosols by the two-way coupled  
1083 WRF-CMAQ over the eastern United States, in *Air Pollution Modeling and its Applications*,  
1084 edited by D. G. Steyn and S. T. Castelli, XXI, Springer Netherlands, Netherlands, C(96), 579–  
1085 583, 2011.
- 1086 Yu, S., Mathur, R., Pleim, J., Wong, D., Gilliam, R., Alapaty, K., Zhao, C., and Liu, X.: Aerosol  
1087 indirect effect on the grid-scale clouds in the two-way coupled WRF–CMAQ: Model  
1088 description, development, evaluation and regional analysis, *Atmos. Chem. Phys.*, 14, 11247–  
1089 11285, <https://doi.org/10.5194/acp-14-11247-2014>, 2014.
- 1090 Yu, S., Li, P., Wang, L., Wu, Y., Wang, S., Liu, W., Zhu, T., Zhang, Y., Hu, M., Alapaty, K.,  
1091 Wong, D., Pleim, J., Mathur, R., Rosenfeld, D., and Seinfeld, J.: Mitigation of severe urban haze  
1092 pollution by a precision air pollution control approach, *Scientific Reports*, 8:8151,  
1093 doi:10.1038/s41598-018-26344-1, 2018.



- 1094 Yu, X.-Y., Lee, T., Ayres, B., Kreidenweis, S. M., Malm, W., and Collett, J. L.: Loss of fine  
1095 particle ammonium from denuded nylon filters, *Atmos. Environ.*, 40, 4797-4807, 2006.
- 1096 Zhang, Y.: Online coupled meteorology and chemistry models: History, current status, and  
1097 outlook, *Atmos. Chem. Phys.*, 8, 2895-2932, doi:10.5194/acp-8-2895-2008, 2008.
- 1098 Zhang, Y. and Wang, K.: Project 3 - Air quality and climate modeling: Multi-model application,  
1099 evaluation, intercomparison, and ensemble over the U.S., poster presentation at the Air Climate  
1100 Energy (ACE) Centers Meeting, Pittsburgh, PA, June 18-19, 2019.
- 1101 Zhang, K. M., Knipping, E. M., Wexler, A. S., Bhawe, P. V., and Tonnesen, G. S.: Size  
1102 distribution of sea-salt emissions as a function of relative humidity, *Atmos. Environ.*, 39, 3373-  
1103 3379, 2005.
- 1104 Zhang, Y., Liu, P., Pun, B, and Seigneur, C.: A comprehensive performance evaluation of MM5-  
1105 CMAQ for the summer 1999 Southern Oxidants Study episode, Part-I. Evaluation protocols,  
1106 databases and meteorological predictions, *Atmos. Environ.*, 40, 4825-4838,  
1107 doi:10.1016/j.atmosenv.2005.12.043, 2006.
- 1108 Zhang, Y., Vijayaraghavan, K., Wen, X.-Y., Snell, H. E., and Jacobson, M. Z.: Probing into  
1109 regional ozone and particulate matter pollution in the United States: 1. A 1-year CMAQ  
1110 simulation and evaluation using surface and satellite data, *J. Geophys. Res.*, 114, D22304,  
1111 doi:10.1029/2009JD011898, 2009a.
- 1112 Zhang, Y., Wen, X.-Y., Wang, K., Vijayaraghavan, K., and Jacobson, M. Z.: Probing into  
1113 regional ozone and particulate matter pollution in the United States: 2. An examination of  
1114 formation mechanisms through a process analysis technique and sensitivity study, *J. Geophys.*  
1115 *Res.*, 114, D22305, doi:10.1029/2009JD011900, 2009b.
- 1116 Zhang, Y., Wen, X.-Y., and Jang C. J.: Simulating chemistry-aerosol-cloud-radiation-climate  
1117 feedbacks over the continental US using the online-coupled Weather Research Forecasting  
1118 Model with chemistry (WRF/Chem), *Atmos. Environ.*, 44(29), 3568-3582, doi:  
1119 10.1016/j.atmosenv.2010.05.056, 2010.
- 1120 Zhang, Y., Sartelet, K., Zhu, S., Wang, W., Wu, S.-Y., Zhang, X., Wang, K., Tran, P., Seigneur,  
1121 C., and Wang, Z.-F.: Application of WRF/Chem-MADRID and WRF/Polyphemus in Europe –  
1122 Part 2: Evaluation of chemical concentrations and sensitivity simulations, *Atmos. Chem. Phys.*,  
1123 13, 6845–6875, https://doi.org/10.5194/acp-13-6845-2013, 2013.
- 1124 Zhang, Y., Chen, Y., Fan, J., and Leung, L. R.: Application of an online-coupled regional  
1125 climate model, WRF-CAM5, over East Asia for examination of ice nucleation schemes: Part II.  
1126 Sensitivity to ice nucleation parameterizations and dust emissions, *Climate*, 3(3), 753-774,  
1127 doi:10.3390/cli3030753, 2015a.
- 1128 Zhang, Y., Zhang, X., Wang, K., He, J., Leung, L. R., Fan, J.-W., and Nenes, A.: Incorporating  
1129 an advanced aerosol activation parameterization into WRF-CAM5: Model evaluation and  
1130 parameterization intercomparison, *J. Geophys. Res.*, 120 (14), doi:10.1002/2014JD023051,  
1131 2015b.



- 1132 Zhang, Y., Zhang, X., Wang, L., Zhang, Q., Duan, F., and He, K.: Application of WRF/Chem  
1133 over East Asia: Part I. Model evaluation and intercomparison with MM5/CMAQ, *Atmos.*  
1134 *Environ.*, 124, 285–300, 2016a.
- 1135 Zhang, Y., Hong, C.-P., Yahya, K., Li, Q., Zhang, Q., and He, K.-B.: Comprehensive evaluation  
1136 of multi-year real-time air quality forecasting using an online-coupled meteorology-chemistry  
1137 model over southeastern United States, *Atmos. Environ.*, 138, 162-182,  
1138 doi:10.1016/j.atmosenv.2016.05.006, 2016b.
- 1139 Zhang, Y., Wang, K., and He J.: Multi-year application of WRF-CAM5 over East Asia-Part II:  
1140 Interannual variability, trend analysis, and aerosol indirect effects, *Atmos. Environ.*, 165, 222-  
1141 239, 2017.
- 1142 Zhang, Y., Jena, C., Wang, K., Paton-Walsh, C., Guérette, E.-A., Utembe, S., Silver, J. D., and  
1143 Keywood, M.: Multiscale applications of two online-coupled meteorology-chemistry models  
1144 during recent field campaigns in Australia, Part I: Model description and WRF/Chem-ROMS  
1145 evaluation using surface and satellite data and sensitivity to spatial grid resolutions, *Atmosphere*,  
1146 10(4), 189, doi:10.3390/atmos10040189, 2019.
- 1147 Zheng, B., Zhang, Q., Zhang, Y., He, K. B., Wang, K., Zheng, G. J., Duan, F. K., Ma, Y. L., and  
1148 Kimoto, T.: Heterogeneous chemistry: a mechanism missing in current models to explain  
1149 secondary inorganic aerosol formation during the January 2013 haze episode in North China,  
1150 *Atmos. Chem. Phys.*, 15, 2031–2049, <https://doi.org/10.5194/acp-15-2031-2015>, 2015.



Table 1. The 5-year (2008-2012) average performance statistics for meteorological variables between two-way WRF-CMAQ and WRF-only simulations.

Variables	Datasets	Mean Obs	Two-way WRF-CMAQ					WRF-only				
			Mean Sim	R	MB	NMB (%)	RMSE	Mean Sim	R	MB	NMB (%)	RMSE
T2 (°C)		12.9	13.0	0.98	0.1	0.8	1.0	13.1	0.98	0.2	1.8	1.1
RH2 (%)	NCDC	69.1	71.3	0.88	2.2	3.2	5.3	71.0	0.88	1.8	2.6	5.2
WS10 (m s <sup>-1</sup> )		3.74	4.18	0.52	0.44	11.7	1.15	4.20	0.52	0.46	12.4	1.16
WD10 (deg)		154.4	187.2	0.07	32.8	21.3	47.7	187.8	0.06	33.4	21.6	48.1
		1.84	2.55	0.62	0.71	38.4	1.27	2.64	0.62	0.8	43.5	1.33
Precipitation (mm day <sup>-1</sup> )	NADP	2.66	2.81	0.84	0.15	5.8	0.7	2.9	0.84	0.24	9.3	0.73
	GPCP	2.15	2.43	0.79	0.28	13.0	0.9	2.45	0.80	0.30	14.1	0.9
	PRISM	2.16	2.30	0.91	0.14	6.8	0.55	2.36	0.91	0.20	9.5	0.56
	TMPA	2.28	2.50	0.86	0.22	9.9	0.81	2.52	0.86	0.24	10.7	0.82
SWDOWN (W m <sup>-2</sup> )		185.6	209.8	0.97	24.2	13.0	25.7	222.6	0.96	37.0	19.9	38.3
GSW (W m <sup>-2</sup> )		158.5	176.0	0.97	17.6	11.1	19.8	187.0	0.95	28.5	18.0	30.6
GLW (W m <sup>-2</sup> )	CERES	322.9	316.8	0.99	-6.1	-1.9	8.1	312.3	0.99	-10.6	-3.3	12.1
OLR (W m <sup>-2</sup> )		241.2	243.2	0.99	2.0	0.8	3.5	244.0	0.99	2.8	1.2	4.2
SWCF (W m <sup>-2</sup> )		-41.1	-30.4	0.74	-10.7	-26.0	13.7	-23.5	0.63	-17.6	-42.8	20.1
LWCF (W m <sup>-2</sup> )		23.7	18.4	0.73	-5.3	-22.2	6.5	17.8	0.74	-5.9	-24.9	6.9
AOD		0.15	0.05	0.60	-0.1	-64.8	0.11	N/A	N/A	N/A	N/A	N/A
CF		0.57	0.50	0.92	-0.07	-12.2	0.09	N/A	N/A	N/A	N/A	N/A
CDNC (cm <sup>-3</sup> )	MODIS	163.3	29.3	0.35	-134.0	-82.1	138.8	N/A	N/A	N/A	N/A	N/A
CWP (g m <sup>-2</sup> )		167.4	81.6	0.79	-85.8	-51.2	90.4	N/A	N/A	N/A	N/A	N/A
COT		15.3	3.0	0.84	-12.3	-80.1	12.6	N/A	N/A	N/A	N/A	N/A

\*outputs of AOD, CF, CDNC, CWP, and COT are not available from WRF-only simulations



Table 2. The 5-year (2008-2012) average performance statistics for chemical variables between two-way WRF-CMAQ and offline CMAQ simulations.

Variables	Datasets	Mean Obs	Two-way WRF-CMAQ					Offline CMAQ				
			Mean Sim	R	MB	NMB (%)	NME (%)	Mean Sim	R	MB	NMB (%)	NME (%)
Max 8-hr O <sub>3</sub> (ppb)	AQS	43.5	49.0	0.66	5.5	12.6	13.1	51.2	0.66	7.7	17.7	17.9
	CASTNET	42.2	42.8	0.65	0.6	1.5	8.4	45.1	0.65	3.0	7.0	10.5
PM <sub>2.5</sub> (µg m <sup>-3</sup> )	CSN	10.7	9.9	0.50	-0.75	-7.0	21.9	10.3	0.46	-0.36	-3.4	21.7
	IMPROVE	4.78	4.13	0.88	-0.65	-13.7	26.6	4.51	0.87	-0.27	-5.7	23.2
PM <sub>10</sub> (µg m <sup>-3</sup> )	AQS	24.0	13.0	0.02	-11.0	-45.9	49.6	15.4	0.14	-8.6	-35.6	45.0
	CSN	2.32	1.70	0.88	-0.62	-26.7	27.1	1.57	0.89	-0.75	-32.3	32.3
SO <sub>4</sub> <sup>2-</sup> (µg m <sup>-3</sup> )	IMPROVE	1.08	0.78	0.98	-0.29	-27.2	27.2	0.76	0.98	-0.32	-29.4	29.4
	CSN	1.29	1.51	0.85	0.22	16.6	32.8	1.73	0.85	0.43	33.5	44.9
NO <sub>3</sub> <sup>-</sup> (µg m <sup>-3</sup> )	IMPROVE	0.41	0.47	0.85	0.06	14.6	42.9	0.57	0.87	0.16	39.0	51.7
	CSN	1.03	0.88	0.86	-0.15	-14.3	18.6	0.87	0.85	-0.16	-15.7	18.7
EC (µg m <sup>-3</sup> )	CSN	0.63	0.76	0.34	0.13	20.6	52.4	0.77	0.39	0.14	22.4	50.5
	IMPROVE	0.18	0.23	0.80	0.05	29.4	50.8	0.25	0.79	0.07	37.7	55.6
OC (µg m <sup>-3</sup> )	IMPROVE	0.97	0.69	0.59	-0.28	-28.9	44.8	0.74	0.58	-0.23	-23.8	43.4
	CSN	2.87	2.60	0.10	-0.27	-9.4	29.7	2.71	0.07	-0.16	-5.7	28.8
TC (µg m <sup>-3</sup> )	IMPROVE	0.68	0.62	0.79	-0.06	-9.2	37.2	0.80	0.72	-0.08	-9.2	39.0
	MOPITT	1.96	1.44	0.89	-0.52	-26.6	26.7	1.45	0.89	-0.51	-26.2	26.2
TOR (DU)	OMI	30.3	30.8	0.83	0.47	1.6	4.7	31.1	0.82	0.77	2.5	5.1
Col. NO <sub>2</sub> (10 <sup>15</sup> mole. cm <sup>-3</sup> )	SCIAMACHY	1.27	1.09	0.91	-0.18	-14.5	27.1	1.08	0.91	-0.19	-14.9	27.3
Col. HCHO (10 <sup>15</sup> mole. cm <sup>-3</sup> )	SCIAMACHY	5.13	4.21	0.83	-0.92	-18.0	20.6	4.28	0.83	-0.85	-16.6	19.8

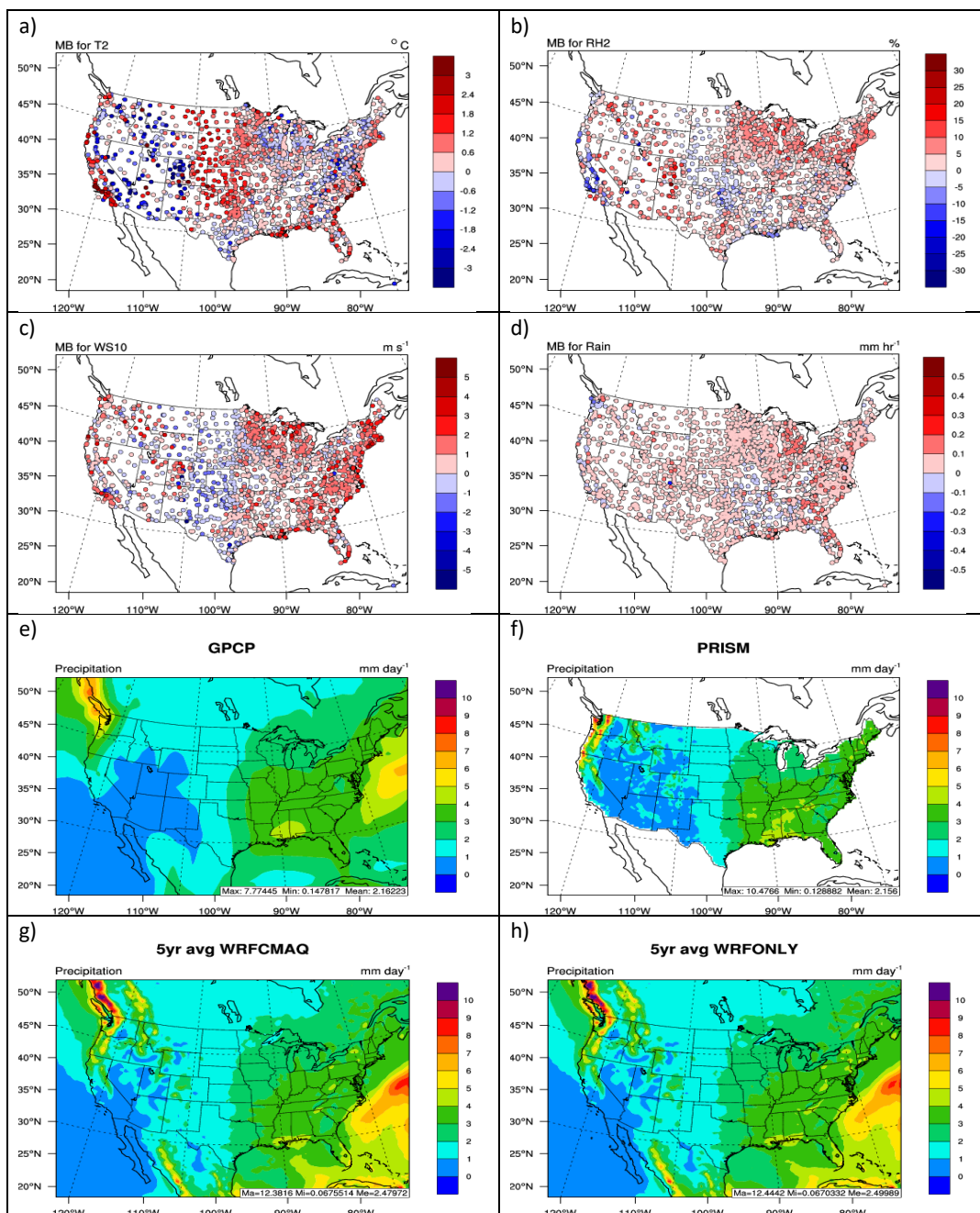


Figure 1. Spatial distributions of 5-year average MBs for a) 2-m temperature (T2), b) 2-m relative humidity (RH2), c) 10-m wind speed (WS10), and d) hourly precipitation from NCDC for two-way WRF-CMAQ in 2008-2012 and 5-year average of daily precipitation for e) GPCP, f) PRISM, g) two-way WRF-CMAQ, and h) WRF-only.

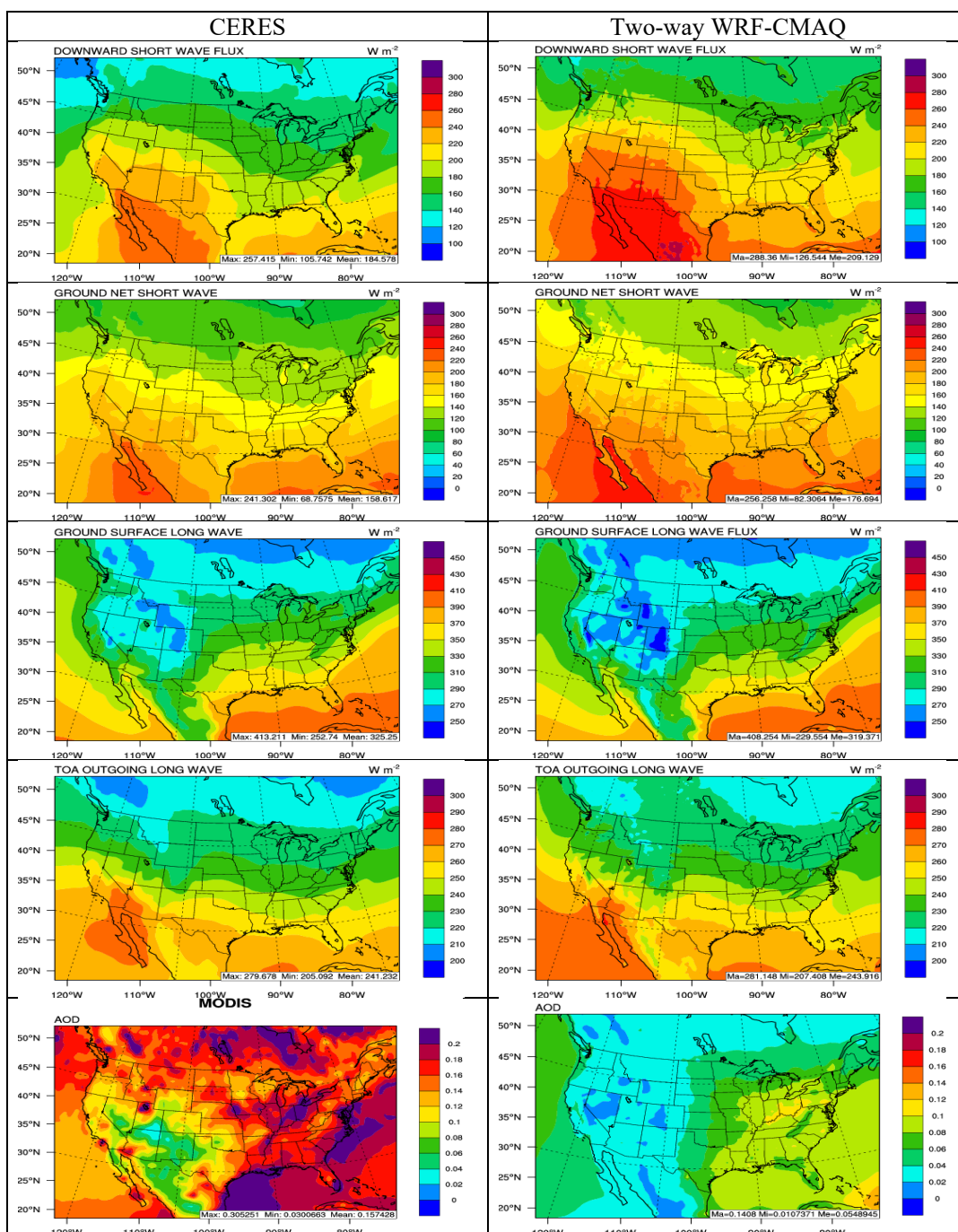


Figure 2. Spatial distribution of 5-year average major radiation variables (from top to bottom: SWDOWN, GSW, GLW, OLR, and AOD) between CERES observations (left panel) vs. two-way WRF-CMAQ (right panel) for 2008-2012.

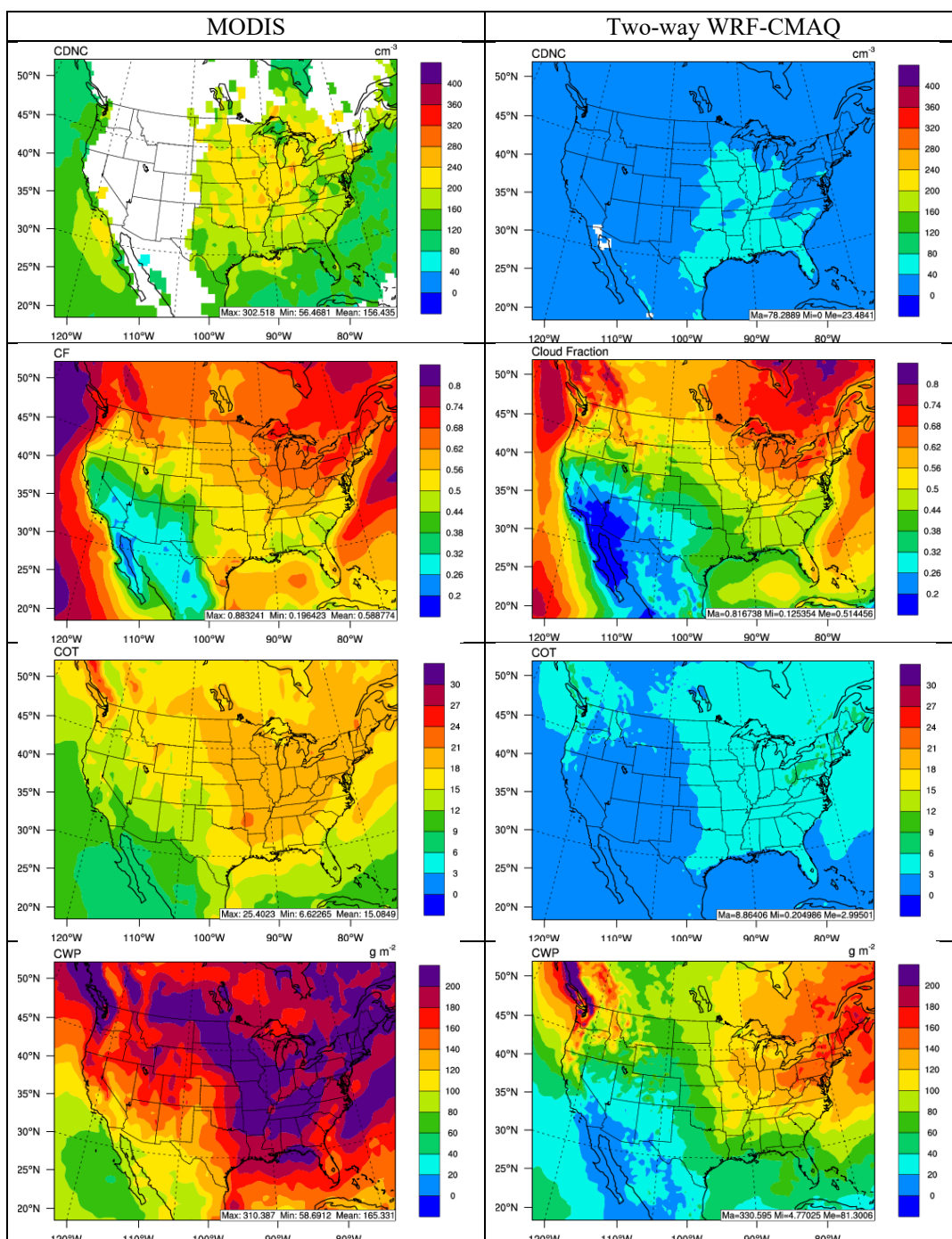


Figure 3. Spatial distribution of 5-year average major cloud variables (from top to bottom: CDNC, CF, COT, and CWP) between MODIS observations (left panel) vs. two-way WRF-CMAQ (right panel) for 2008-2012.

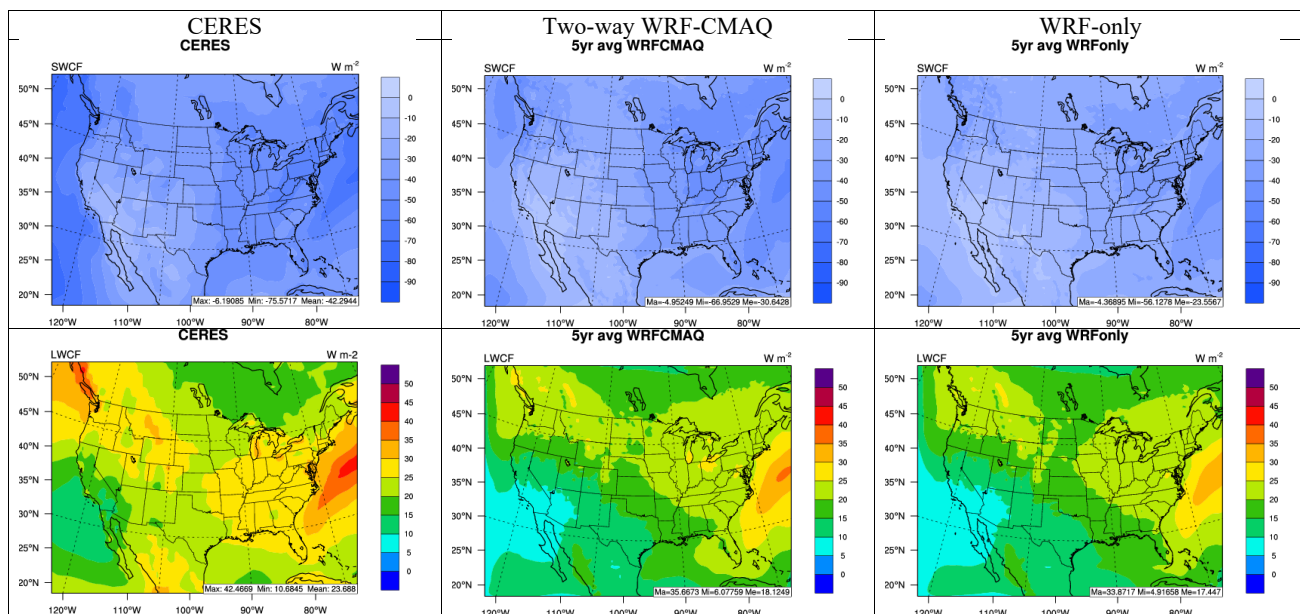


Figure 4. Spatial distribution of 5-year average SWCF (top panel) and LWCF (bottom panel) between CERES observations (left panel) vs. two-way WRF-CMAQ (center panel) and WRF-only (right panel) for 2008-2012.

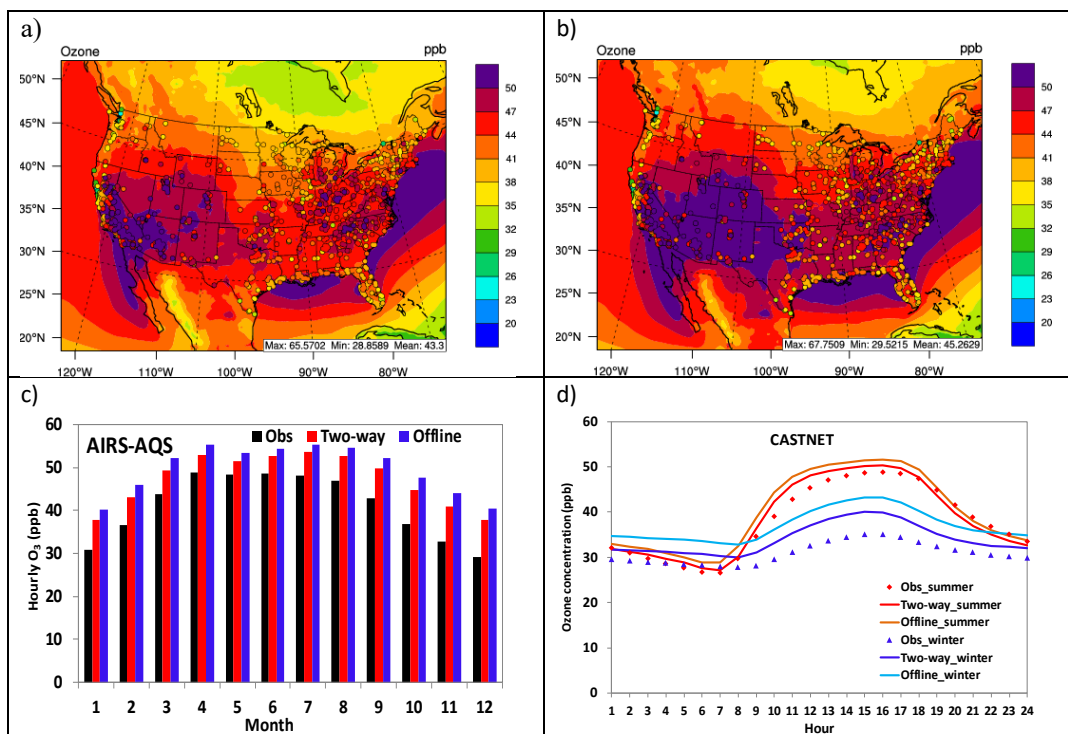


Figure 5. Spatial distributions of 5-year averaged max 8-h  $O_3$  overlaid with observations from AIRS-AQS and CASTNET for a) two-way WRF-CMAQ and b) offline CMAQ; c) bar chart for 5-year average monthly  $O_3$  between observations (black bar), two-way WRF-CMAQ (red bar), and offline CMAQ (blue bar); and d) diurnal plots of observed (dots) vs. simulated (lines) hourly  $O_3$  concentrations against CASTNET for winter (cold colors) and summer (warm colors) in 2008-2012.

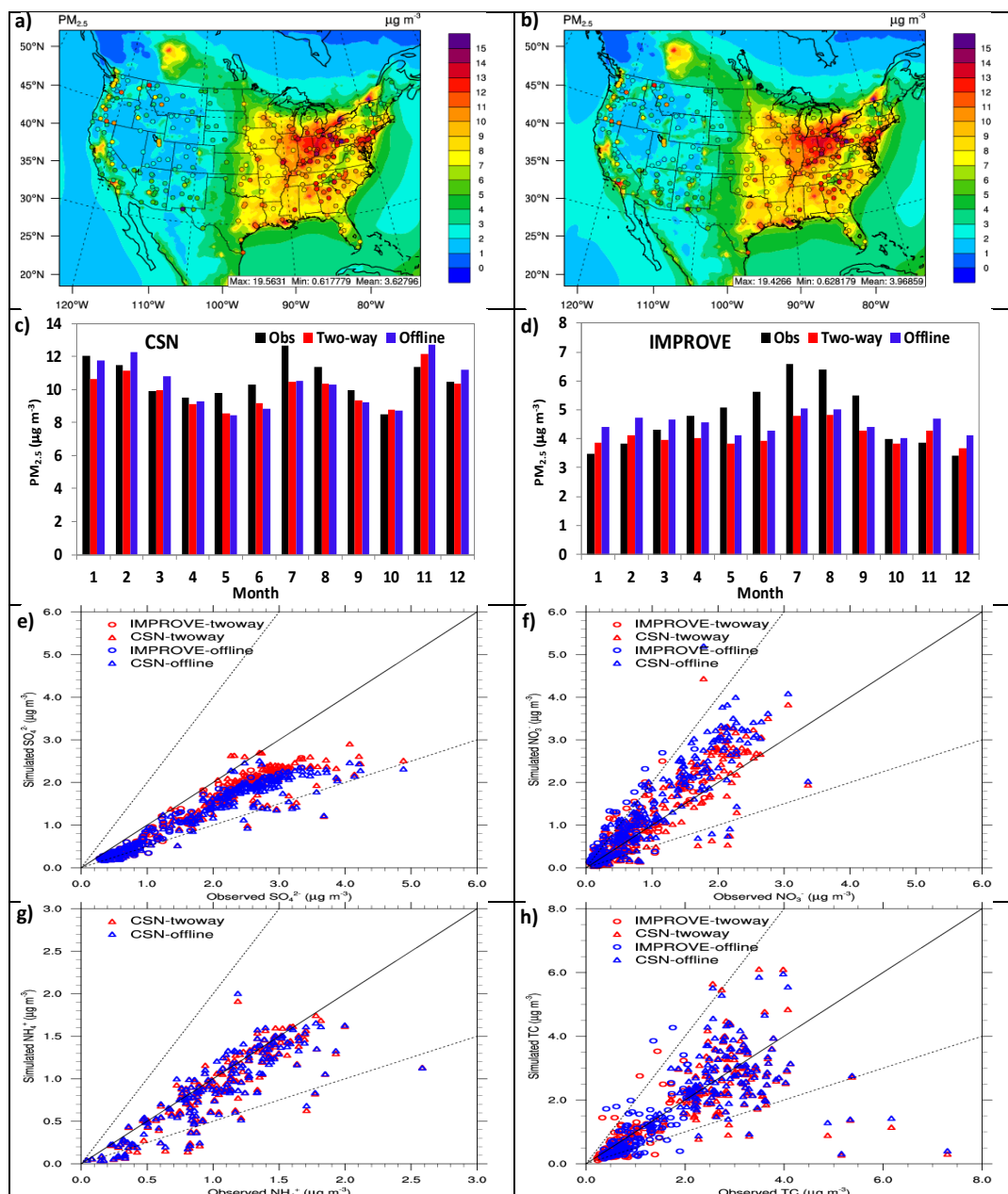


Figure 6. Spatial distributions of 5-year averaged daily  $PM_{2.5}$  overlaid with observations from CSN and IMPROVE for a) two-way WRF-CMAQ and b) offline CMAQ; bar charts for 5-year average monthly  $PM_{2.5}$  between observations (black bar), two-way WRF-CMAQ (red bar), and offline CMAQ (blue bar) over c) CSN and d) IMPROVE; and scatter plots of  $PM_{2.5}$  constituents e)  $SO_4^{2-}$ , f)  $NH_4^+$ , g)  $NO_3^-$ , and h) TC) between observations and simulations of two-way WRF-CMAQ (red color) and offline CMAQ (blue) for 2008–2012.

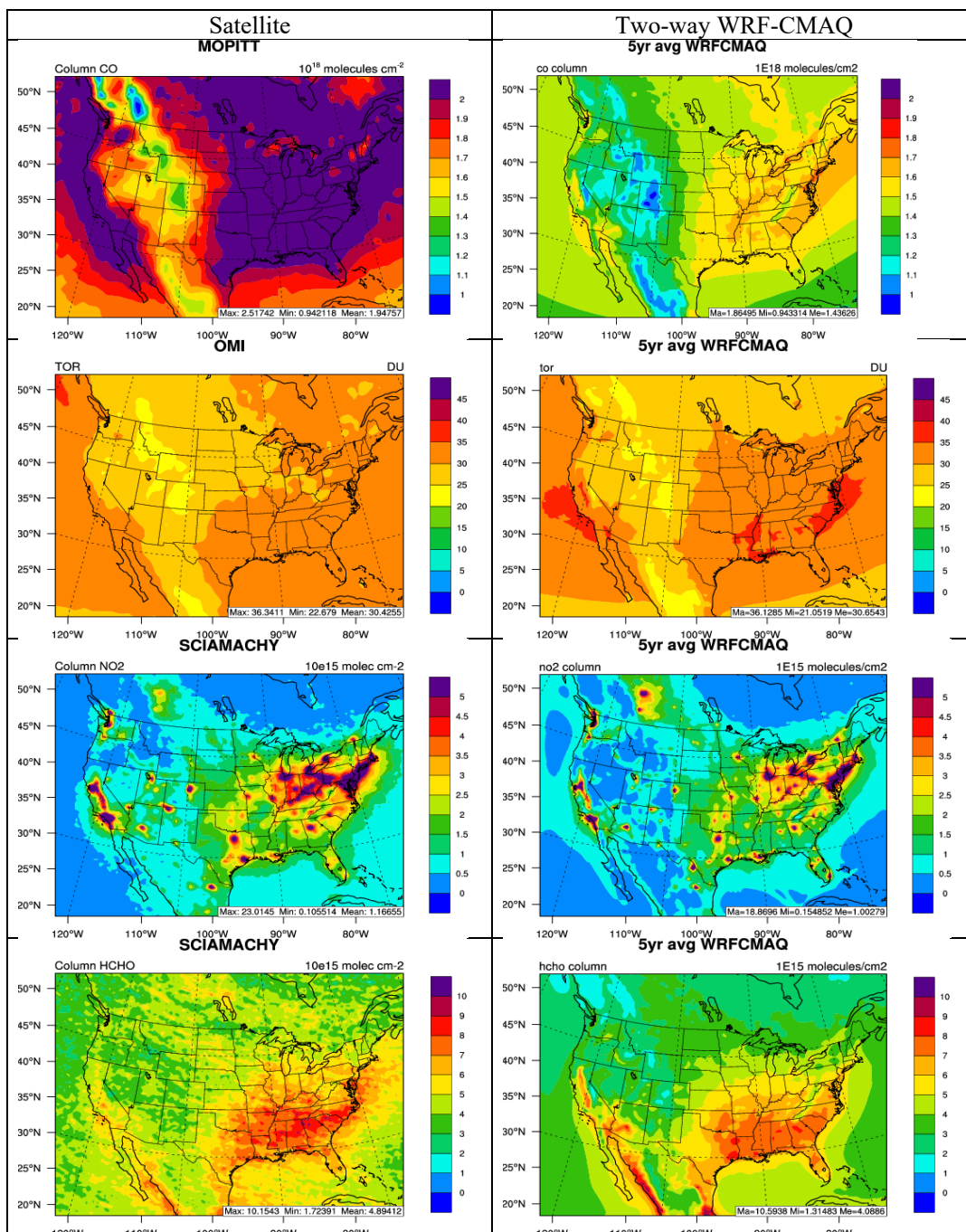


Figure 7. Spatial distribution of 5-year average column abundances (from top to bottom: column CO, TOR, column NO<sub>2</sub>, and column HCHO) between various satellite observations (left panel) vs. two-way WRF-CMAQ (right panel) for 2008-2012.

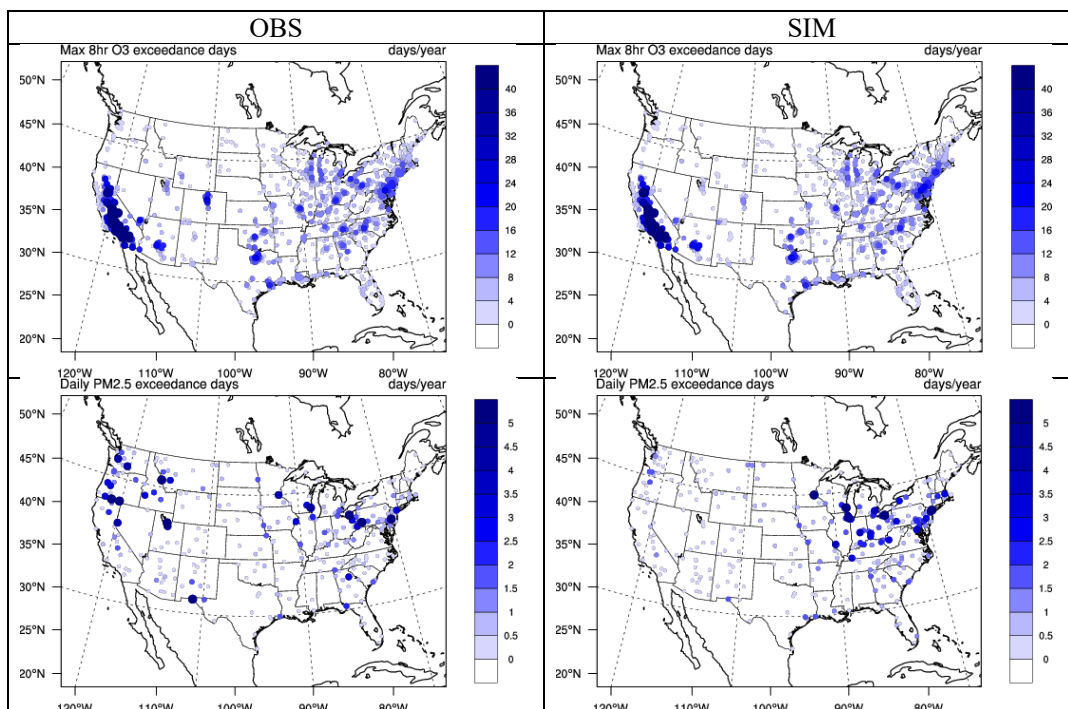


Figure 8. The spatial distribution of 5-year average annual exceedance days of max 8-h O<sub>3</sub> and daily PM<sub>2.5</sub> between observations (O<sub>3</sub> over the AIRS-AQS/CASTNET network and PM<sub>2.5</sub> over the IMPROVE/CSN network) and two-way WRF-CMAQ.

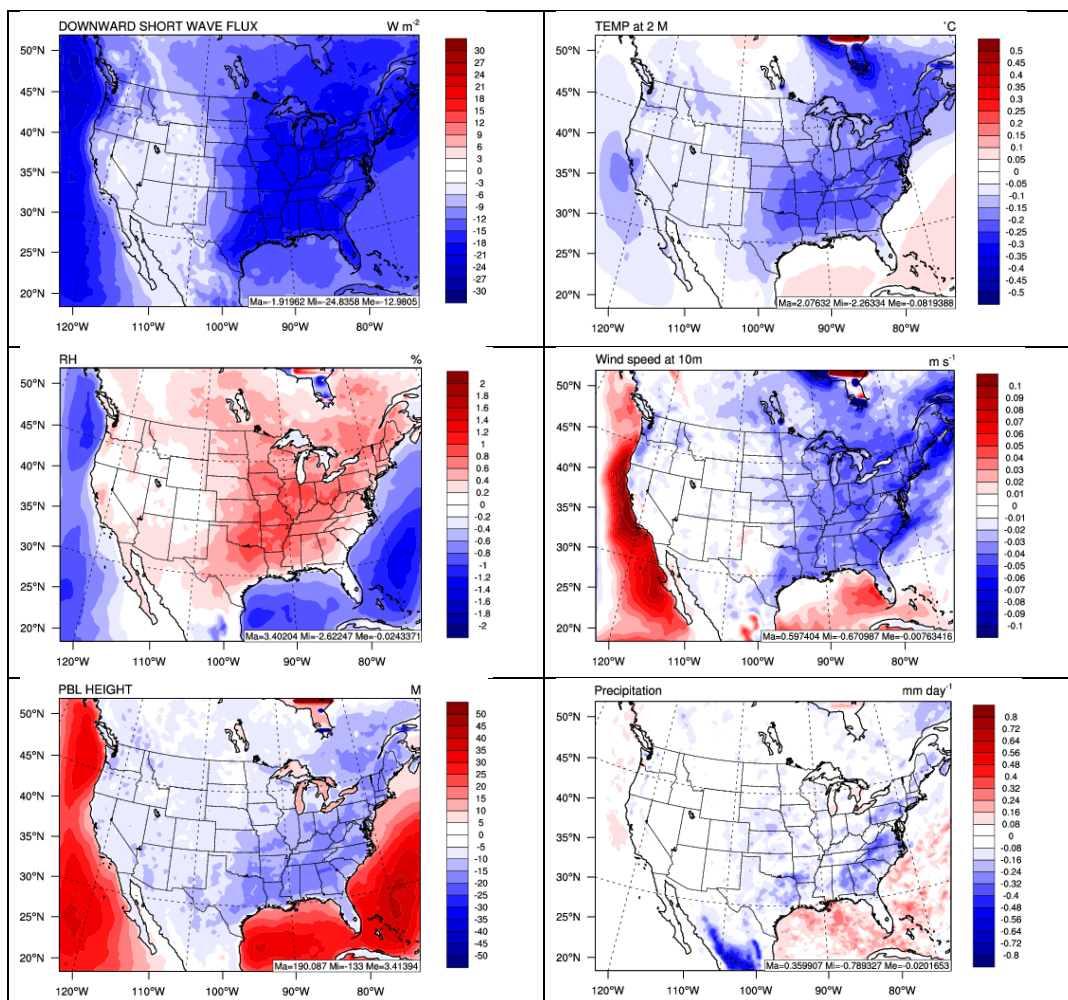


Figure 9. Spatial difference plots (two-way WRF-CMAQ - WRF-only) for major meteorological variables between two-way WRF-CMAQ and WRF-only.

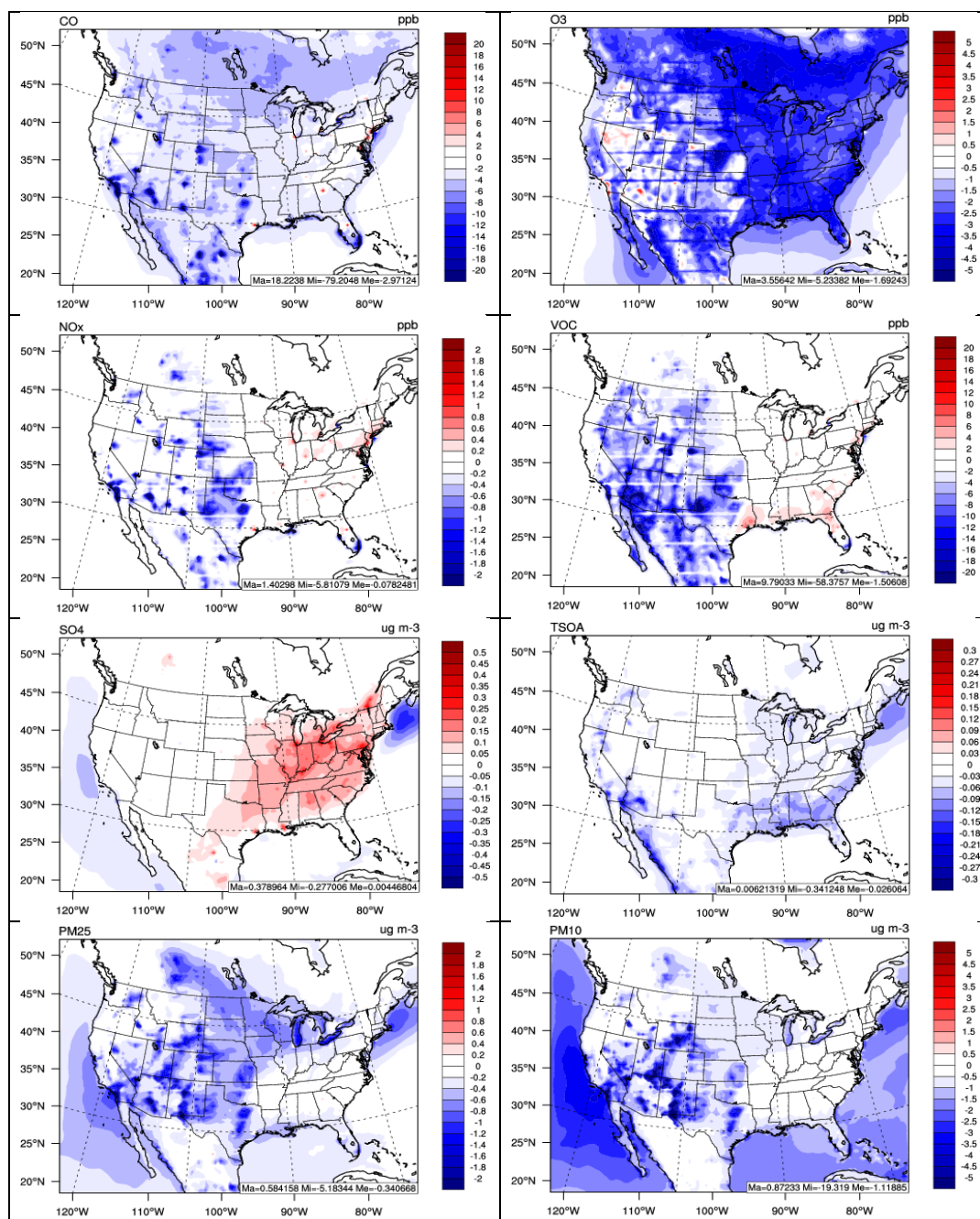


Figure 10. Spatial difference plots (two-way WRF-CMAQ - offline CMAQ) for major chemical species between two-way WRF-CMAQ and offline CMAQ.